

Robust kernel-free quadratic surface twin support vector machine with capped L_1 -norm distance metric

Qi Si^{a,b}, Zhixia Yang^{a,b,*}

^a*College of Mathematics and Systems Science, Xinjiang University, Urumuqi 830046, China*

^b*Institute of Mathematics and Physics, Xinjiang University, Urumuqi 830046, China*

Abstract

Twin support vector machine (TSVM) is a very classical and practical classifier for pattern classification. However, the traditional TSVM has two limitations. Firstly, it uses the L_2 -norm distance metric that leads to its sensitivity to outliers. Second, it needs to select the appropriate kernel function and the kernel parameters for nonlinear classification. To effectively avoid these two problems, this paper proposes a robust capped L_1 -norm kernel-free quadratic surface twin support vector machine (CL₁QTSVM). The strengths of our model are briefly summarized as follows. 1) The robustness of our model is further improved by employing the capped L_1 norm distance metric. 2) Our model is a kernel-free method that avoids the time-consuming process of selecting appropriate kernel functions and kernel parameters. 3) The introduction of L_2 -norm regularization term to improve the generalization ability of the model. 4) To efficiently solve the proposed model, an iterative algorithm is developed. 5) The convergence, time complexity and existence of locally optimal solutions of the developed algorithms are further discussed. Numerical experiments on numerous types of datasets validate the classification performance and robustness of the proposed model.

Keywords: Capped L_1 -norm, Robust classification, Kernel-free trick, Twin support vector machine, Iterative algorithms.

*Corresponding authors

Email address: yangzhx@xju.edu.cn (Zhixia Yang)

1. Introduction

With the development of data science, the processing and learning of data is increasingly important. In view of the strong generalization ability of the support vector machine (SVM) (Hearst et al., 1998) and its following the principle of structural risk minimization (SRM), which leads to its increasing application in classification and regression learning tasks (Xie et al., 2023b; Gupta et al., 2020). In addition, the classical SVM deal with nonlinear classification problems by introducing suitable kernel functions (Cortes and Vapnik, 1995). Nowadays, SVM models have been widely applied in the fields of fault diagnosis (Ma et al., 2018), pattern classification (Xie et al., 2023b), gene expression (Brown et al., 2000), face recognition (Noble, 2004), and text classification (Goh et al., 2005).

However, the classical SVM model can be limited to handle certain data distributions, such as the XOR problem. In addition, traditional SVMs obtain the optimal solutions of the primal problem by solving a quadratic programming problem (QPP), which leads to some limitations in dealing with large-scale problems. To address the above two problems, twin SVM (TSVM) has been proposed (Chandra and Khemchandani, 2007). In comparison to classical SVMs, traditional TSVM solve two smaller size quadratic programming problems (QPPs), which leads to its computational speed theoretically to be faster than that of SVMs. The classical TSVM only considers the empirical risk minimization principle and not the SRM principle. Therefore, to make TSVM follow the SRM principle, Shao et al. proposed twin bounded SVM (TBSVM) by introducing a regularization term in the TSVM model (Shao et al., 2011). In recent years, the TSVM model has been further improved and applied to the fields of robust classification learning (Si et al., 2023), multi-view data classification (Xie and Xiong, 2022), unbalanced data classification (Moosaei et al., 2023) and deep learning (Xie et al., 2023a).

Recently, some scholars have proposed numerous improvements by combining kernel-free techniques with SVM and TSVM models. The kernel-free soft-margin quadratic surface support vector machine (SQSSVM) was first proposed by Luo *et al.* for the binary classification problem (Luo et al., 2016). Similarly, Bai *et al.* proposed quadratic least squares support vector machine (QLSSVM) (Bai et al., 2015). Subsequently, Gao et al. proposed quadratic TSVM (QTTSVM) and quadratic least squares TSVM model (LSQTTSVM) by combining kernel-free techniques with TSVM (Gao et al., 2019). In order to make QSSVM deal with high-dimensional feature problems effectively, Gao *et*

al. proposed ν -version fuzzy reduced SQSSVM (ν -FRSQSSVM) (Gao et al., 2022). In recent years, the double well potential (DWP) function, which is a 4th order polynomial function, has also been studied more and more extensively(Gao and Yu, 2008; Xia et al., 2014; Gao et al., 2021b,a). Although the above kernel-free methods improve the performance of SVM and TSVM models for nonlinear classification problems, they have not been applied to the field of robust classification learning, and thus this is an extendable research direction.

Although TSVM has achieved good performance in pattern classification, there is still room for improvement. The main reason for this is that TSVM uses the L_2 norm distance metric and the hinge loss function, which causes it to be sensitive to outliers or noises (Borah and Gupta, 2020; Zheng et al., 2021). In order to enhance the robustness of the model, some scholars have proposed many improvements based on the distance norm. For instance, Wang *et al.* combined the capped L_1 -norm distance metric with TSVM (CTSVM) to deal with robust classification problems (Wang et al., 2019). In order to make CTSVM follow the SRM principle, Ma *et al.* proposed capped L_1 -norm distance metric-based fast robust TBSVM (FRTBSVM) by introducing a regularization term in the CTSVM model (Ma et al., 2020). Similarly, Yuan *et al.* introduced the new capped $L_{2,p}$ norm metric in the least squares TSVM model (Yuan and Yang, 2021). Recently, Wang *et al.* also introduced capped $L_{2,p}$ norm metric and bounded Welsch loss function into TSVM (Wang et al., 2023). In addition, the capped L_1 -norm distance metric has been introduced into methods such as the twin extreme learning machines (CL_1 TEL) (Ma, 2020) and the twin projection extreme learning machines (CL_1 TPELM) (Yang et al., 2023). It can be seen that the above methods improve the robustness of TSVM, but they are not combined with kernel-free techniques, which is very interesting.

Noting that no scholars have combined capped L_1 -norm distance metric with kernel-free TSVM to solve robust classification problems until now, this paper proposes a new kernel-free quadratic surface TSVM model based on capped L_1 -norm distance metric. Our model is to find two quadratic surfaces such that each surface is as close to one class of points and as far away from the other class of points as possible. The main contributions of the paper are summarized as follows:

- The robustness of the LSQTSVM model to outliers is improved by introducing capped L_1 -norm loss.

- To comply with the structural risk minimization (SRM) principle, we introduce a regularization term to improve the generalization ability of model.
- And efficient and fast iterative algorithms are developed to solve the optimization problem of proposed models.
- The convergence, time complexity and existence of optimal solutions of our algorithm are analyzed theoretically to further validate the effectiveness of our CL_1 QTSVM model.
- Experiments on synthetic and real datasets validate that the proposed CL_1 QTSVM model slightly outperforms the compared state-of-the-art methods in terms of robustness.

The remaining parts of this paper are summarized as follows. Section 2 briefly reviews the work related to this paper, including some definitions, models and norms. Section 3 presents our model and its corresponding solution algorithm. Furthermore, some further theoretical analysis of the algorithm is provided. Section 4 shows the results of numerical experiments on synthetic and real datasets. Section 5 briefly summarizes the contributions of this paper and future work.

2. Related work

In this section, we first introduce some notations and double well potential functions used in the paper. Then, some related models and distance metrics are briefly reviewed.

2.1. Notation

Throughout this paper, scalars, vectors and matrices are represented in italics. Furthermore, scalars are not required to be bolded, while vectors and matrices are required to be bolded. \mathbb{R}^n and \mathbb{R}_+^n denote the n -dimensional real number space and the n -dimensional non-negative real space respectively. \mathbb{S}^n and \mathbb{D}^n represent the real symmetric and real diagonal matrices of $n \times n$, respectively. The $\mathbf{0}$ means a zero matrix of appropriate dimension, while \mathbf{I} represents a identity matrix of arbitrary dimension. All vectors used in this paper default to column vectors. \top indicates a transpose operation. \mathbf{e}_+ and \mathbf{e}_- represent m_+ and m_- dimensional all-one column vectors, respectively.

For a binary dataset \mathcal{T} , it can be formulated mathematically as follows

$$\mathcal{T} = \left\{ (\mathbf{x}_i^\pm, y_i^\pm)_{i=1,2,\dots,m_\pm} \mid \mathbf{x}_i^\pm \in \mathbb{R}^n, y_i^\pm \in \{+1, -1\} \right\}, \quad (1)$$

where $m = m_+ + m_-$, m_+ and m_- represent the number of positive and negative sample points, respectively. Furthermore, n represents the feature dimension of the data \mathbf{x} . Meanwhile, the positive and negative sample matrices are defined as $\mathbf{X}_+ = [\mathbf{x}_1^+, \dots, \mathbf{x}_{m_+}^+]^\top \in \mathbb{R}^{m_+ \times n}$ and $\mathbf{X}_- = [\mathbf{x}_1^-, \dots, \mathbf{x}_{m_-}^-]^\top \in \mathbb{R}^{m_- \times n}$, respectively.

Then, we briefly introduce the four vectorization operators employed in this paper, which are extensively used in kernel-free SVM, TSVM models (Gao et al., 2022, 2021a). For any $\mathbf{A} \in \mathbb{S}^n$, its semi-vectorized operator follows

$$\begin{aligned} \text{hvec}(\mathbf{A}) &\triangleq [A_{11}, \dots, A_{1n}, A_{22}, \dots, A_{2n}, \dots, A_{n-1,n-1}, A_{n-1,n}, A_{nn}]^\top \\ &\in \mathbb{R}^{n(n+1)/2}. \end{aligned} \quad (2)$$

If $\mathbf{A} \in \mathbb{D}^n$, the diagonal vectorization operator is

$$\text{dvec}(\mathbf{A}) \triangleq [A_{11}, A_{22}, \dots, A_{n-1,n-1}, A_{nn}]^\top \in \mathbb{R}^n. \quad (3)$$

Furthermore, given the vector $\mathbf{x} = [x_1, \dots, x_n]^\top \in \mathbb{R}^n$, its quadratic vectorization operator is defined as follows

$$\text{lvec}(\mathbf{x}) \triangleq \left[\frac{1}{2}x_1^2, x_1x_2, \dots, x_1x_n, \frac{1}{2}x_2^2, x_2x_3, \dots, x_2x_n, \dots, \frac{1}{2}x_n^2 \right]^\top \in \mathbb{R}^{\frac{n(n+1)}{2}}, \quad (4)$$

and its quadratic vectorization operator without cross terms can be defined as follows

$$\text{qvec}(\mathbf{x}) \triangleq \left[\frac{1}{2}x_1^2, \frac{1}{2}x_2^2, \dots, \frac{1}{2}x_n^2 \right]^\top \in \mathbb{R}^n. \quad (5)$$

2.2. Related models

In this subsection, we will briefly review two classical correlation methods called LSQTSVM and FRTBSVM.

2.2.1. LSQTSVM

Recently, kernel-free TSVM methods have been further extensively studied. Gao et al. proposed the least squares quadratic TSVM (LSQTSVM) model (Gao et al., 2019). In particular, the LSQTSVM model solves a pair of quadratic surfaces as follows

$$\frac{1}{2}\mathbf{x}^\top \mathbf{A}_\pm \mathbf{x} + \mathbf{b}_\pm^\top \mathbf{x} + c_\pm = 0, \quad (6)$$

where $\mathbf{A}_\pm \in \mathbb{S}^n$, $\mathbf{b}_\pm \in \mathbb{R}^n$, $c_\pm \in \mathbb{R}$.

To obtain the above pair of quadratic surfaces (6), the LSQTSVM model is built as follows

(LSQTSVM1)

$$\begin{aligned} & \min \frac{1}{2} \sum_{i=1}^{m_+} \left(\frac{1}{2} \mathbf{x}_i^{+\top} \mathbf{A}_+ \mathbf{x}_i^+ + \mathbf{b}_+^\top \mathbf{x}_i^+ + c_+ \right)^2 + C \sum_{j=1}^{m_-} (\xi_j^-)^2, \\ & \text{s.t. } -\left(\frac{1}{2} \mathbf{x}_j^{-\top} \mathbf{A}_+ \mathbf{x}_j^- + \mathbf{b}_+^\top \mathbf{x}_j^- + c_+ \right) = 1 - \xi_j^-, \quad j = 1, 2, \dots, m_-, \\ & \mathbf{A}_+ \in \mathbb{S}^n, \mathbf{b}_+ \in \mathbb{R}^n, c_+ \in \mathbb{R}, \boldsymbol{\xi}_- \in \mathbb{R}^{m_-}. \end{aligned} \tag{7}$$

and

(LSQTSVM2)

$$\begin{aligned} & \min \frac{1}{2} \sum_{j=1}^{m_-} \left(\frac{1}{2} \mathbf{x}_j^{-\top} \mathbf{A}_- \mathbf{x}_j^- + \mathbf{b}_-^\top \mathbf{x}_j^- + c_- \right)^2 + C \sum_{i=1}^{m_+} (\xi_i^+)^2, \\ & \text{s.t. } \frac{1}{2} \mathbf{x}_i^{+\top} \mathbf{A}_- \mathbf{x}_i^+ + \mathbf{b}_-^\top \mathbf{x}_i^+ + c_- = 1 - \xi_i^+, \quad i = 1, 2, \dots, m_+, \\ & \mathbf{A}_- \in \mathbb{S}^n, \mathbf{b}_- \in \mathbb{R}^n, c_- \in \mathbb{R}, \boldsymbol{\xi}_+ \in \mathbb{R}^{m_+}. \end{aligned} \tag{8}$$

where C is a given positive parameter. $\boldsymbol{\xi}_+ = [\xi_1^+, \dots, \xi_{m_+}^+]^\top \in \mathbb{R}^{m_+}$, $\boldsymbol{\xi}_- = [\xi_1^-, \dots, \xi_{m_-}^-]^\top \in \mathbb{R}^{m_-}$. Take the objective function of the optimization problem (7) as an example and briefly introduce the constructive idea. Its first term is to make the positive points as close as possible to the positive quadratic surface $\frac{1}{2} \mathbf{x}^\top \mathbf{A}_+ \mathbf{x} + \mathbf{x}^\top \mathbf{b}_+ + c_+$, and its second term is to measure the loss of each negative point by the square loss function. The optimization problems (7) and (8) can be equivalently transformed by the definitions (2) and (4), then the corresponding solutions are obtained, as detailed in Ref(Gao et al., 2019).

If the solutions \mathbf{A}_\pm , \mathbf{b}_\pm and c_\pm of the optimization problems (7) and (8) are obtained, then the label of a new sample \mathbf{x} can be predicted by the following decision rule

$$\text{Class } \mathbf{x} = \operatorname{argmin}_{k=+,-} \left\{ \frac{\left| \frac{1}{2} \mathbf{x}^\top \mathbf{A}_k \mathbf{x} + \mathbf{x}^\top \mathbf{b}_k + c_k \right|}{\|\mathbf{A}_k \mathbf{x} + \mathbf{b}_k\|_2} \right\}. \tag{9}$$

2.2.2. FRTBSVM

As we all know the traditional TSVM model is lower than the classical SVM model in terms of computational consumption. However, the TSVM model uses the L_2 distance metric and hinge loss to increase the effect of outliers on the classifier. To improve this limitation of TSVM, Ma *et al.* proposed a robust and fast TBSVM model based on the capped L_1 -norm distance metric called FRTBSVM (Ma et al., 2020).

For a given binary dataset \mathcal{T} (1), the kernel version of FRTBSVM tries to find the following pair of hyperplanes

$$\mathbf{u}_\pm^\top \mathbf{x} + b_\pm = 0, \quad (10)$$

where $\mathbf{u}_\pm \in \mathbb{R}^n$, $b_\pm \in \mathbb{R}$.

To find two hypersurfaces (10), the kernel version of the FRTBSVM model is presented as follows

(CL₁FRTBSVM1)

$$\begin{aligned} & \min \sum_{i=1}^{m_+} \min (|\mathbf{u}_+^\top \mathbf{x}_i^+ + b_+|, \varepsilon) + \frac{c}{2} (\|\mathbf{u}_+\|_2^2 + b_+^2) + C \sum_{j=1}^{m_-} \min (|\eta_j^-|, \varepsilon) \\ \text{s.t. } & -(\mathbf{X}_- \mathbf{u}_+ + \mathbf{e}_- b_+) = \mathbf{e}_- - \boldsymbol{\eta}_-, \\ & \mathbf{u}_+ \in \mathbb{R}^n, b_+ \in \mathbb{R}, \boldsymbol{\eta}_- \in \mathbb{R}^{m_-}, \end{aligned} \quad (11)$$

and

(CL₁FRTBSVM2)

$$\begin{aligned} & \min \sum_{j=1}^{m_-} \min (|\mathbf{u}_-^\top \mathbf{x}_j^- + b_-|, \varepsilon) + \frac{c}{2} (\|\mathbf{u}_-\|_2^2 + b_-^2) + C \sum_{i=1}^{m_+} \min (|\eta_i^+|, \varepsilon) \\ \text{s.t. } & -(\mathbf{X}_+ \mathbf{u}_- + \mathbf{e}_+ b_-) = \mathbf{e}_+ - \boldsymbol{\eta}_+, \\ & \mathbf{u}_- \in \mathbb{R}^n, b_- \in \mathbb{R}, \boldsymbol{\eta}_+ \in \mathbb{R}^{m_+}, \end{aligned} \quad (12)$$

where c and C are known regularization parameters. The optimization problems (11) and (12) can be solved efficiently by an iterative algorithm. Specific details of the solution process and optimization problem formulation can be found in paper (Ma et al., 2020). If we obtain the solutions \mathbf{u}_\pm and b_\pm , then the label of a new sample can be obtained by the following decision rule

$$\text{Class } \mathbf{x} = \operatorname{argmin}_{k=+,-} \{|\mathbf{u}_\pm^\top \mathbf{x} + b_\pm|\}. \quad (13)$$

2.3. Capped L_1 -norm

As mentioned in the introduction, the capped L_1 -norm loss is effective in reducing the effect of outliers on the classifier(Yan et al., 2018; Wu et al., 2017; Xiang et al., 2012; Nie et al., 2014). Because outliers in the data usually have large errors, the capped L_1 -norm usually helps the model filter out these points during the training process. However, using the capped L_1 -norm distance metric usually results in the model becoming a non-smooth problem. Furthermore, the mathematical formulation of the capped L_1 -norm loss is shown as follows

$$L_\epsilon(u) = \min(|u|, \epsilon), \quad (14)$$

where ϵ is a given parameter, $\epsilon = 0.5$ in Figure 1.

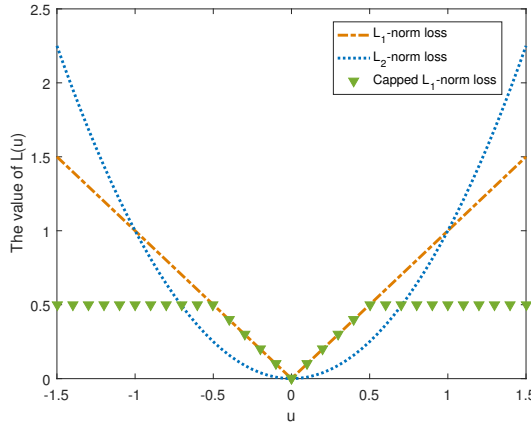


Figure 1: The geometric interpretations of different norm metrics

Figure 1 illustrates some geometric variations of the distance norm. As shown in Figure 1, compared with the traditional L_1 -norm loss and L_2 -norm loss, the value of capped L_1 -norm loss will remain constant when $u > \epsilon$. In other words, the capped L_1 -norm loss can be used to measure noises and outliers. Therefore, capped L_1 -norm loss is more robust than L_1 -norm loss and L_2 -norm loss.

3. The proposed method

In this section, we first introduce the capped L_1 -norm quadric TSVM (CL₁QTSVM). Then, to solve the proposed models efficiently, we design fast

iterative algorithms for it. Finally, we also analyze convergence, computational complexity and local optimal solutions of the algorithm in detail.

3.1. CL_1 QTSVM

For a given training set \mathcal{T} (1), our goal is to also find two quadratic surfaces (6), thus the mathematical expression for our CL_1 QTSVM model is as follows

(CL_1 QTSVM1)

$$\begin{aligned}
& \min \sum_{i=1}^{m_+} \min \left(\left| \frac{1}{2} \mathbf{x}_i^{+\top} \mathbf{W}_+ \mathbf{x}_i^+ + \mathbf{b}_+^\top \mathbf{x}_i^+ + c_+ \right|, \varepsilon \right) + \frac{1}{2} c_1 (\| \text{hvec}(\mathbf{W}_+) \|_2^2 + \| \mathbf{b}_+ \|_2^2 + c_+^2) \\
& \quad + c_2 \sum_{j=1}^{m_-} \min (|\eta_j^-|, \varepsilon), \\
& \text{s.t. } - \left(\frac{1}{2} \mathbf{x}_j^{-\top} \mathbf{W}_+ \mathbf{x}_j^- + \mathbf{b}_+^\top \mathbf{x}_j^- + c_+ \right) = 1 - \eta_j^-, \quad j = 1, 2, \dots, m_-, \\
& \quad \mathbf{W}_+ \in \mathbb{S}^n, \mathbf{b}_+ \in \mathbb{R}^n, c_+ \in \mathbb{R}, \boldsymbol{\eta}_- \in \mathbb{R}^{m_-},
\end{aligned} \tag{15}$$

and

(CL_1 QTSVM2)

$$\begin{aligned}
& \min \sum_{j=1}^{m_-} \min \left(\left| \frac{1}{2} \mathbf{x}_j^{-\top} \mathbf{W}_- \mathbf{x}_j^- + \mathbf{b}_-^\top \mathbf{x}_j^- + c_- \right|, \varepsilon \right) + \frac{1}{2} c_1 (\| \text{hvec}(\mathbf{W}_-) \|_2^2 + \| \mathbf{b}_- \|_2^2 + c_-^2) \\
& \quad + c_2 \sum_{i=1}^{m_+} \min (|\eta_i^+|, \varepsilon), \\
& \text{s.t. } \frac{1}{2} \mathbf{x}_i^{+\top} \mathbf{W}_- \mathbf{x}_i^+ + \mathbf{b}_-^\top \mathbf{x}_i^+ + c_- = 1 - \eta_i^+, \quad i = 1, 2, \dots, m_+, \\
& \quad \mathbf{W}_- \in \mathbb{S}^n, \mathbf{b}_- \in \mathbb{R}^n, c_- \in \mathbb{R}, \boldsymbol{\eta}_+ \in \mathbb{R}^{m_+},
\end{aligned} \tag{16}$$

where c_1 and c_2 are known regularization parameters. ε is a small values that is set to 10^{-5} in our experiments.

In the established CL_1 -QTSVM model, the capped L_1 -norm distance metric is used to weaken the effect of outliers on the kernel-free quadratic dual support vector machine model. Taking the objective function of the optimization problem (15) as an example, we briefly introduce its construction

principle. The first term of the objective function of the optimization problem (15) is to make the positive points as close as possible to the positive quadratic decision hypersurface $\frac{1}{2}\mathbf{x}^\top \mathbf{W}_+ \mathbf{x} + \mathbf{x}^\top \mathbf{b}_+ + c_+$. If the modulus of this positive point to a positive quadratic decision hypersurface is larger than ε , then set its metric to ε . The second term of the objective function of the optimization problem (15) is the L_2 norm regularization term, which is used to improve the generalization ability of our model as well as to avoid the problem of non-existence of matrix inverses during the solution process. The third term of the objective function for the optimization problem (15) is the loss term, whose value is determined by the location of the negative points. If the modulus of a negative point to a positive quadratic proximal hypersurface satisfies $|\frac{1}{2}\mathbf{x}_j^\top \mathbf{W}_+ \mathbf{x}_j^- + \mathbf{b}_+^\top \mathbf{x}_j^- + c_+ + 1| > \varepsilon$, the loss of the negative class point is set to ε . This helps to minimize the effect of outliers in the negative points on the positive quadratic decision hypersurfaces. The objective function of the optimization problem (16) is built in a similar way and is not described here.

To further solve the optimization problems (15) and (16), we define the following equations

$$\mathbf{w}_\pm \triangleq [\text{hvec}^\top(\mathbf{W}_\pm), \mathbf{b}_\pm^\top, c_\pm]^\top \in \mathbb{R}^{\frac{n^2+3n+2}{2}}, \quad (17)$$

$$\mathbf{z}_i^+ \triangleq \left[\text{lvec}^\top(\mathbf{x}_i^+), \mathbf{x}_i^{+\top}, 1 \right]^\top, \in \mathbb{R}^{\frac{n^2+3n+2}{2}}, i = 1, 2, \dots, m_+, \quad (18)$$

$$\mathbf{z}_j^- \triangleq \left[\text{lvec}^\top(\mathbf{x}_j^-), \mathbf{x}_j^{-\top}, 1 \right]^\top, \in \mathbb{R}^{\frac{n^2+3n+2}{2}}, j = 1, 2, \dots, m_-. \quad (19)$$

By the definition of Eqs. (17)-(19), we simplify the above two optimization problems as follows

(CL₁QTSVM1)

$$\begin{aligned} \min \quad & \sum_{i=1}^{m_+} \min(|\mathbf{w}_+^\top \mathbf{z}_i^+|, \varepsilon) + \frac{1}{2} c_1 \|\mathbf{w}_+\|_2^2 + c_2 \sum_{j=1}^{m_-} \min(|\eta_j^-|, \varepsilon), \\ \text{s.t.} \quad & -\mathbf{w}_+^\top \mathbf{z}_j^- = 1 - \eta_j^-, \quad j = 1, 2, \dots, m_-, \\ & \mathbf{w}_+ \in \mathbb{R}^{\frac{n^2+3n+2}{2}}, \boldsymbol{\eta}_- \in \mathbb{R}^{m_-}, \end{aligned} \quad (20)$$

and

(CL₁QTSVM2)

$$\begin{aligned} \min \quad & \sum_{j=1}^{m_-} \min (|\mathbf{w}_-^\top \mathbf{z}_j^+|, \varepsilon) + \frac{1}{2} c_1 \|\mathbf{w}_-\|_2^2 + c_2 \sum_{i=1}^{m_+} \min (|\eta_i^+|, \varepsilon), \\ \text{s.t.} \quad & \mathbf{w}_-^\top \mathbf{z}_i^+ = 1 - \eta_i^+, \quad i = 1, 2, \dots, m_+, \\ & \mathbf{w}_- \in \mathbb{R}^{\frac{n^2+3n+2}{2}}, \boldsymbol{\eta}_+ \in \mathbb{R}^{m_+}, \end{aligned} \quad (21)$$

Furthermore, we note that it is difficult to solve the above optimization problems (20) and (21) by conventional convex optimization methods. By employing the re-weighted trick (Yan et al., 2018; Wu et al., 2017; Xiang et al., 2012), we can reformulate the above two optimization problems into the following two approximate optimization problems

(CL₁QTSVM1)

$$\min_{\mathbf{w}_+, \boldsymbol{\eta}_-} \frac{1}{2} (\mathbf{G}_+^\top \mathbf{w}_+)^T \mathbf{Q} \mathbf{G}_+^\top \mathbf{w}_+ + \frac{1}{2} c_1 \|\mathbf{w}_+\|_2^2 + \frac{1}{2} c_2 \boldsymbol{\eta}_-^\top \mathbf{U} \boldsymbol{\eta}_-, \quad (22)$$

where $\mathbf{Z}_+ \triangleq [\mathbf{z}_1^+, \dots, \mathbf{z}_{m_+}^+] \in \mathbb{R}^{(\frac{n^2+3n+2}{2}) \times m_+}$, and $\mathbf{Z}_- \triangleq [\mathbf{z}_1^-, \dots, \mathbf{z}_{m_-}^-] \in \mathbb{R}^{(\frac{n^2+3n+2}{2}) \times m_-}$. $\mathbf{Q} \in \mathbb{R}^{m_+ \times m_+}$ and $\mathbf{U} \in \mathbb{R}^{m_- \times m_-}$ are two diagonal matrices whose diagonal elements are defined as

$$q_i = \begin{cases} \frac{1}{|\mathbf{w}_+^\top \mathbf{z}_i^+|}, & |\mathbf{w}_+^\top \mathbf{z}_i^+| \leq \varepsilon, \\ \varepsilon, & \text{otherwise.} \end{cases}, \quad (23)$$

and

$$u_j = \begin{cases} \frac{1}{|\eta_j^-|}, & |\eta_j^-| \leq \varepsilon, \\ \varepsilon, & \text{otherwise.} \end{cases}. \quad (24)$$

(CL₁QTSVM2)

$$\min_{\mathbf{w}_-, \boldsymbol{\eta}_+} \frac{1}{2} (\mathbf{G}_-^\top \mathbf{w}_-)^T \mathbf{F} \mathbf{G}_-^\top \mathbf{w}_- + \frac{1}{2} c_1 \|\mathbf{w}_-\|_2^2 + \frac{1}{2} c_2 \boldsymbol{\eta}_+^\top \mathbf{G} \boldsymbol{\eta}_+, \quad (25)$$

where $\mathbf{F} \in \mathbb{R}^{m_- \times m_-}$ and $\mathbf{G} \in \mathbb{R}^{m_+ \times m_+}$ are two diagonal matrices whose diagonal elements are defined as

$$f_j = \begin{cases} \frac{1}{|\mathbf{w}_-^\top \mathbf{z}_j^-|}, & |\mathbf{w}_-^\top \mathbf{z}_j^-| \leq \varepsilon, \\ \varepsilon, & \text{otherwise.} \end{cases}, \quad (26)$$

and

$$g_i = \begin{cases} \frac{1}{|\eta_i^+|}, & |\eta_i^+| \leq \varepsilon, \\ \varepsilon, & \text{otherwise.} \end{cases} \quad (27)$$

Remark 1. It is worth noting that in the objective function of the optimization problem (22), the matrices \mathbf{Q} and \mathbf{U} are used to “discard” outliers from the data. If positive points are far from the positive decision quadratic surface, then these points are considered positive outliers and are discarded. Similarly, if negative points are far from the positive proximal quadratic surface, they are also considered negative outliers and are excluded. The matrices \mathbf{F} and \mathbf{G} are interpreted similarly.

To solve the optimization problems (22) and (25), we first equivalently convert them into the following form

$$\begin{aligned} (\text{CL}_1\text{QTSVM1}) \min_{\mathbf{w}_+} J_+(\mathbf{w}_+) &\triangleq \frac{1}{2} (\mathbf{Z}_+^\top \mathbf{w}_+)^{\top} \mathbf{Q} \mathbf{Z}_+^\top \mathbf{w}_+ + \frac{1}{2} c_1 \|\mathbf{w}_+\|_2^2 \\ &\quad + \frac{1}{2} c_2 (\mathbf{Z}_-^\top \mathbf{w}_+ + \mathbf{e}_-)^{\top} \mathbf{U} (\mathbf{Z}_-^\top \mathbf{w}_+ + \mathbf{e}_-), \end{aligned} \quad (28)$$

and

$$\begin{aligned} (\text{CL}_1\text{QTSVM2}) \min_{\mathbf{w}_-} J_-(\mathbf{w}_-) &\triangleq \frac{1}{2} (\mathbf{Z}_-^\top \mathbf{w}_-)^{\top} \mathbf{F} \mathbf{Z}_-^\top \mathbf{w}_- + \frac{1}{2} c_1 \|\mathbf{w}_-\|_2^2 \\ &\quad + \frac{1}{2} c_2 (\mathbf{e}_+ - \mathbf{Z}_+^\top \mathbf{w}_-)^{\top} \mathbf{G} (\mathbf{e}_+ - \mathbf{Z}_+^\top \mathbf{w}_-). \end{aligned} \quad (29)$$

And to obtain the gradient for the optimization problems (28) and (29) and to set them to zero, we have

$$\nabla J_+(\mathbf{w}_+) = \mathbf{Z}_+ \mathbf{Q} \mathbf{Z}_+^\top \mathbf{w}_+ + c_1 \mathbf{I} \mathbf{w}_+ + c_2 \mathbf{Z}_- \mathbf{U} (\mathbf{Z}_-^\top \mathbf{w}_+ + \mathbf{e}_-) = \mathbf{0}, \quad (30)$$

and

$$\nabla J_-(\mathbf{w}_-) = \mathbf{Z}_- \mathbf{F} \mathbf{Z}_-^\top \mathbf{w}_- + c_1 \mathbf{I} \mathbf{w}_- - c_2 \mathbf{Z}_+ \mathbf{G} (\mathbf{e}_+ - \mathbf{Z}_+^\top \mathbf{w}_-) = \mathbf{0}. \quad (31)$$

To obtain the final iterative equations, we first define the following equations

$$\mathbf{M}_-^t \triangleq \mathbf{Y}^t - \mathbf{Y}^t \mathbf{Z}_- \left(\frac{1}{c_2} (\mathbf{U}^t)^{-1} + \mathbf{Z}_-^\top \mathbf{Y}^t \mathbf{Z}_- \right)^{-1} \mathbf{Z}_-^\top \mathbf{Y}^t, \quad (32)$$

$$\mathbf{Y}^t \triangleq \frac{1}{c_1} \left(\mathbf{I} - \mathbf{Z}_+ \left(c_1 \mathbf{Q}^t + \mathbf{Z}_+^\top \mathbf{Z}_+ \right)^{-1} \mathbf{Z}_+^\top \right), \quad (33)$$

$$\mathbf{M}_+^t \triangleq \mathbf{H}^t - \mathbf{H}^t \mathbf{Z}_+ \left(\frac{1}{c_2} (\mathbf{G}^t)^{-1} + \mathbf{Z}_+^\top \mathbf{H}^t \mathbf{Z}_+ \right)^{-1} \mathbf{Z}_+^\top \mathbf{H}^t, \quad (34)$$

$$\mathbf{H}^t \triangleq \frac{1}{c_1} \left(\mathbf{I} - \mathbf{Z}_- \left(c_1 \mathbf{F}^t + \mathbf{Z}_-^\top \mathbf{Z}_- \right)^{-1} \mathbf{Z}_-^\top \right). \quad (35)$$

And then based on Eqs. (30)-(35) and Sherman-Morrison-Woodbury (SMW) theorem (Kumar and Gopal, 2009), we propose the following iterative formulas with respect to the variables \mathbf{w}_+ and \mathbf{w}_-

$$\mathbf{w}_+^{t+1} = \begin{cases} -c_2 \mathbf{M}_-^\top \mathbf{Z}_- \mathbf{U}^t \mathbf{e}_-, & \frac{n^2+3n+2}{2} > m_-, \\ -c_2 (\mathbf{Z}_+ \mathbf{Q}^t \mathbf{Z}_+^\top + c_1 \mathbf{I} + c_2 \mathbf{Z}_- \mathbf{U}^t \mathbf{Z}_-^\top)^{-1} \mathbf{Z}_- \mathbf{U}^t \mathbf{e}_-, & \text{otherwise,} \end{cases}, \quad (36)$$

and

$$\mathbf{w}_-^{t+1} = \begin{cases} c_2 \mathbf{M}_+^\top \mathbf{Z}_+ \mathbf{G}^t \mathbf{e}_+, & \frac{n^2+3n+2}{2} > m_+, \\ c_2 (\mathbf{Z}_- \mathbf{F}^t \mathbf{Z}_-^\top + c_1 \mathbf{I} + c_2 \mathbf{Z}_+ \mathbf{G}^t \mathbf{Z}_+^\top)^{-1} \mathbf{Z}_+ \mathbf{G}^t \mathbf{e}_+, & \text{otherwise,} \end{cases}. \quad (37)$$

where t is the iteration number. By given initial values \mathbf{w}_+^0 and \mathbf{w}_-^0 , the iterative process works by repeating Eqs. (36) and (37) until convergence. Thus, if solutions \mathbf{w}_+ and \mathbf{w}_- are obtained, the two quadratic surfaces (6) are also found. For a new sample \mathbf{x} , its label can be predicted by the decision function (9).

Then we briefly summarize the pseudo-code algorithmic framework for the CL₁QTSVM1 model as follows, and the algorithm for the CL₁QTSVM2 model is similar.

3.2. Convergence analysis

In this subsection we analyze the convergence of the proposed Algorithm 1 in detail. In particular, the convergence of Algorithm 1 is given by Theorem 1. To further prove Theorem 1 in detail, we first give the following lemma 1.

Lemma 1. *For any non-negative variables $x, y \in \mathbb{R}_+$, the following inequality holds:*

$$\sqrt{x} - \frac{x}{2\sqrt{y}} \leq \sqrt{y} - \frac{y}{2\sqrt{y}}. \quad (38)$$

Proof. According to the inequality $(\sqrt{x} - \sqrt{y})^2 \geq 0$, we have

$$\begin{aligned} (\sqrt{x} - \sqrt{y})^2 \geq 0 &\Rightarrow x - 2\sqrt{xy} + y \geq 0 \Rightarrow \sqrt{x} - \frac{x}{2\sqrt{y}} \leq \frac{\sqrt{y}}{2} \\ &\Rightarrow \sqrt{x} - \frac{x}{2\sqrt{y}} \leq \sqrt{y} - \frac{y}{2\sqrt{y}}. \end{aligned} \quad (39)$$

Algorithm 1 CL₁QTSVM1

Require: Training set \mathcal{T} (1), convergence precision $\epsilon = 10^{-8}$, maximum iteration number $N = 30$, parameter c_1, c_2 , threshold parameter $\varepsilon = 10^{-8}$, model parameter $\mathbf{w}_+^0 = \mathbf{0}_{(\frac{n^2+3n+2}{2}) \times 1}$, iteration number $t = 0$.

Ensure: $\mathbf{W}_+, \mathbf{b}_+, c_+$.

```

1:  $\mathbf{z}_i^+ \triangleq [\text{hvec}^\top(\mathbf{x}_i), \mathbf{x}_i^\top, 1]^\top, \mathbf{z}_j^- \triangleq [\text{hvec}^\top(\mathbf{x}_j), \mathbf{x}_j^\top, 1]^\top.$ 
2:  $\mathbf{Z}_+ \triangleq [\mathbf{z}_1^+, \dots, \mathbf{z}_{m_+}^+], \mathbf{Z}_- \triangleq [\mathbf{z}_1^-, \dots, \mathbf{z}_{m_-}^-].$ 
3: while  $t \leq N$  do
4:   for  $i \leftarrow 1$  to  $m_+$  do
5:     if  $|\mathbf{z}_i^{+\top} \mathbf{w}_+^t| \leq \varepsilon$  then
6:        $z_i^t \leftarrow \frac{1}{|\mathbf{z}_i^{+\top} \mathbf{w}_+^t|};$ 
7:     else
8:        $z_i^t \leftarrow \varepsilon.$ 
9:     end if
10:   end for
11:   for  $j \leftarrow 1$  to  $m_-$  do
12:     if  $|1 + \mathbf{z}_j^{-\top} \mathbf{w}_+^t| \leq \varepsilon$  then
13:        $u_j^t \leftarrow \frac{1}{|1 + \mathbf{z}_j^{-\top} \mathbf{w}_+^t|};$ 
14:     else
15:        $u_j^t \leftarrow \varepsilon.$ 
16:     end if
17:   end for
18:    $\mathbf{Y}^t \leftarrow \frac{1}{c_1} \left( \mathbf{I} - \mathbf{Z}_+ \left( c_1 \mathbf{Q}^t + \mathbf{Z}_+^\top \mathbf{Z}_+ \right)^{-1} \mathbf{Z}_+^\top \right).$ 
19:    $\mathbf{M}_-^t \leftarrow \mathbf{Y}^t \mathbf{Z}_- \left( \frac{1}{c_2} (\mathbf{U}^t)^{-1} + \mathbf{Z}_-^\top \mathbf{Y}^t \mathbf{Z}_- \right)^{-1} \mathbf{Z}_-^\top \mathbf{Y}^t.$ 
20:   if  $\frac{n^2+3n+2}{2} > m_-$  then
21:      $\mathbf{w}_+^{t+1} \leftarrow -c_2 \mathbf{M}_-^t \mathbf{Z}_- \mathbf{U}^t \mathbf{e}_-;$ 
22:   else
23:      $\mathbf{w}_+^{t+1} \leftarrow -c_2 \left( \mathbf{Z}_+ \mathbf{Q}^t \mathbf{Z}_+^\top + c_1 \mathbf{I} + c_2 \mathbf{Z}_- \mathbf{U}^t \mathbf{Z}_-^\top \right)^{-1} \mathbf{Z}_- \mathbf{U}^t \mathbf{e}_-.$ 
24:   end if
25:    $t \leftarrow t + 1.$ 
26: end while
27:  $[\text{hvec}^\top(\mathbf{W}_+), \mathbf{b}_+^\top, c_+]^\top \leftarrow \mathbf{w}_+^{t+1}.$ 

```

□

Lemma 2. For any non-negative variables $x, y, z, t, c \in \mathbb{R}_+$, the following inequality holds:

$$\sqrt{x} - \frac{x}{2\sqrt{y}} + c \left(\sqrt{z} - \frac{z}{2\sqrt{t}} \right) \leq \sqrt{y} - \frac{y}{2\sqrt{y}} + c \left(\sqrt{t} - \frac{t}{2\sqrt{t}} \right). \quad (40)$$

Proof. From Lemma 1, the following inequality holds

$$c \left(\sqrt{z} - \frac{z}{2\sqrt{t}} \right) \leq c \left(\sqrt{t} - \frac{t}{2\sqrt{t}} \right). \quad (41)$$

Thus based on Lemma 1 and Eq. (41), we have

$$\sqrt{x} - \frac{x}{2\sqrt{y}} + c \left(\sqrt{z} - \frac{z}{2\sqrt{t}} \right) \leq \sqrt{y} - \frac{y}{2\sqrt{y}} + c \left(\sqrt{t} - \frac{t}{2\sqrt{t}} \right). \quad (42)$$

□

Next, we will prove the convergence of Algorithm 1 based on the optimization problem (15). Similarly, the proposed Algorithm 1 to solve the optimization problem (16) is also convergent.

Theorem 1. Algorithm 1 will decrease the objective value of the optimization problem (15) with each iteration until it converges.

Proof. First recall that the optimization problem (15) is as follows

$$\begin{aligned} J &= \min_{\mathbf{W}_+, \mathbf{b}_+, c_+, \eta_-} \sum_{i=1}^{m_+} \min \left(\left| \frac{1}{2} \mathbf{x}_i^{+\top} \mathbf{W}_+ \mathbf{x}_i^+ + \mathbf{b}_+^\top \mathbf{x}_i^+ + c_+ \right|, \varepsilon \right) + c_2 \sum_{j=1}^{m_-} \min \left(|\eta_j^-|, \varepsilon \right) \\ &\quad + \frac{1}{2} c_1 (\| \text{hvec}(\mathbf{W}_+) \|_2^2 + \| \mathbf{b}_+ \|_2^2 + c_+^2), \\ &= \min_{\mathbf{w}_1^+, \mathbf{w}_2^+, \eta_-} \sum_{i=1}^{m_+} \min \left(\left| \mathbf{w}_1^{+\top} \mathbf{l}_i^+ + \mathbf{w}_2^{+\top} \mathbf{s}_i^+ \right|, \varepsilon \right) + c_2 \sum_{j=1}^{m_-} \min \left(|\eta_j^-|, \varepsilon \right) \\ &\quad + \frac{1}{2} c_1 (\| \mathbf{w}_1^+ \|_2^2 + \| \mathbf{w}_2^+ \|_2^2), \end{aligned} \quad (43)$$

where $\mathbf{w}_1^+ \triangleq \text{hvec}(\mathbf{W}_+) \in \mathbb{R}^{\frac{n^2+n}{2}}, \mathbf{w}_2^+ \triangleq [\mathbf{b}_+^\top, c_+]^\top \in \mathbb{R}^{n+1}, \mathbf{l}_i^+ \triangleq \text{lvec}(\mathbf{x}_i^+) \in \mathbb{R}^{\frac{n^2+n}{2}}, \mathbf{s}_i^+ \triangleq [\mathbf{x}_i^{+\top}, 1]^\top \in \mathbb{R}^{n+1}, i = 1, 2, \dots, m_+$. Note that \mathbf{w}_1^+ contains

nonlinear information in the data, while \mathbf{w}_2^+ contains linear information in the data; when $\mathbf{w}_1^+ = \mathbf{0}$, the optimization problem (15) degenerates to a linear method, which reflects the nonlinear nature of our model.

When $|\mathbf{w}_1^{+\top} \mathbf{l}_i^+ + \mathbf{w}_2^{+\top} \mathbf{s}_i^+| < \varepsilon$ and $|\eta_j^-| < \varepsilon$, Eq. (43) is equivalent to

$$J = \min_{\mathbf{w}_1^+, \mathbf{w}_2^+, \boldsymbol{\eta}_-} \sum_{i=1}^{m_+} |\mathbf{w}_1^{+\top} \mathbf{l}_i^+ + \mathbf{w}_2^{+\top} \mathbf{s}_i^+| + c_2 \sum_{j=1}^{m_-} |\eta_j^-| + \frac{1}{2} c_1 (\|\mathbf{w}_1^+\|_2^2 + \|\mathbf{w}_2^+\|_2^2). \quad (44)$$

We take the derivative of Eq. (44) with respect to \mathbf{w}_1^+ , \mathbf{w}_2^+ and η_j^- separately, we have

$$\begin{aligned} \frac{\partial J}{\partial \mathbf{w}_1^+} = 0 &\Rightarrow \sum_{i=1}^{m_+} \frac{\mathbf{l}_i^+ (\mathbf{l}_i^{+\top} \mathbf{w}_1^+ + \mathbf{s}_i^{+\top} \mathbf{w}_2^+)}{|\mathbf{l}_i^{+\top} \mathbf{w}_1^+ + \mathbf{s}_i^{+\top} \mathbf{w}_2^+|} + c_1 \mathbf{w}_1^+ = \mathbf{0}, \\ \frac{\partial J}{\partial \mathbf{w}_2^+} = 0 &\Rightarrow \sum_{i=1}^{m_+} \frac{\mathbf{s}_i^+ (\mathbf{l}_i^{+\top} \mathbf{w}_1^+ + \mathbf{s}_i^{+\top} \mathbf{w}_2^+)}{|\mathbf{l}_i^{+\top} \mathbf{w}_1^+ + \mathbf{s}_i^{+\top} \mathbf{w}_2^+|} + c_1 \mathbf{w}_2^+ = \mathbf{0}, \\ \frac{\partial J}{\partial \eta_j^-} = 0 &\Rightarrow c_2 \sum_{j=1}^{m_-} \frac{\eta_j^-}{|\eta_j^-|} = 0. \end{aligned} \quad (45)$$

Then combining the above Eqs. (45), we have

$$\begin{aligned} &\sum_{i=1}^{m_+} \frac{\mathbf{l}_i^+ (\mathbf{l}_i^{+\top} \mathbf{w}_1^+ + \mathbf{s}_i^{+\top} \mathbf{w}_2^+)}{|\mathbf{l}_i^{+\top} \mathbf{w}_1^+ + \mathbf{s}_i^{+\top} \mathbf{w}_2^+|} + \sum_{i=1}^{m_+} \frac{\mathbf{s}_i^+ (\mathbf{l}_i^{+\top} \mathbf{w}_1^+ + \mathbf{s}_i^{+\top} \mathbf{w}_2^+)}{|\mathbf{l}_i^{+\top} \mathbf{w}_1^+ + \mathbf{s}_i^{+\top} \mathbf{w}_2^+|} + c_1 (\mathbf{w}_1^+ + \mathbf{w}_2^+) + c_2 \sum_{j=1}^{m_-} \frac{\eta_j^-}{|\eta_j^-|} \\ &= \sum_{i=1}^{m_+} \frac{\mathbf{z}_i^+ \mathbf{z}_i^{+\top} \mathbf{w}_+}{|\mathbf{w}_+^\top \mathbf{z}_i^+|} + c_1 \mathbf{w}_+ + c_2 \sum_{j=1}^{m_-} \frac{\eta_j^-}{|\eta_j^-|} = 0, \end{aligned} \quad (46)$$

where $\mathbf{w}_+ \triangleq [\mathbf{w}_1^{+\top}, \mathbf{w}_2^{+\top}]^\top \in \mathbb{R}^{\frac{n^2+3n+2}{2}}$, $\mathbf{z}_i^+ \triangleq [\mathbf{l}_i^{+\top}, \mathbf{s}_i^{+\top}]^\top \in \mathbb{R}^{\frac{n^2+3n+2}{2}}$.

Then we construct two diagonal matrices \mathbf{Q} and \mathbf{U} , and define $q_i = \frac{1}{|\mathbf{w}_+^\top \mathbf{z}_i^+|}$ and $u_j = \frac{1}{|\eta_j^-|}$ as the diagonal elements of \mathbf{Q} and \mathbf{U} respectively. Rewriting Eq. (46) leads to

$$\mathbf{Z}_+ \mathbf{Q} \mathbf{Z}_+^\top \mathbf{w}_+ + c_1 \mathbf{I} \mathbf{w}_+ + c_2 \mathbf{U} \boldsymbol{\eta}_- = 0. \quad (47)$$

Apparently, Eqs. (47) is the optimal solution to the following optimization problem

$$\min_{\mathbf{w}_+, \boldsymbol{\eta}_-} \frac{1}{2} (\mathbf{Z}_+^\top \mathbf{w}_+)^T \mathbf{Q} \mathbf{Z}_+^\top \mathbf{w}_+ + \frac{1}{2} c_1 \|\mathbf{w}_+\|_2^2 + \frac{1}{2} c_2 \boldsymbol{\eta}_-^\top \mathbf{U} \boldsymbol{\eta}_-. \quad (48)$$

Now, let $\bar{\mathbf{w}}_+ \triangleq \left[\text{hvec}^\top(\bar{\mathbf{W}}_+), \bar{\mathbf{b}}_+^\top, \bar{c}_+ \right]^\top$ and $\bar{\boldsymbol{\eta}}_- \triangleq \mathbf{Z}_-^\top \bar{\mathbf{w}}_+ + \mathbf{e}_-$ represent the updated \mathbf{w}_+ and $\boldsymbol{\eta}_-$ by Eqs. (36). Then it is easy to obtain the following inequality

$$\begin{aligned} & \frac{1}{2} \bar{\mathbf{w}}_+^\top \mathbf{Z}_+ \mathbf{Q} \mathbf{Z}_+^\top \bar{\mathbf{w}}_+ + \frac{1}{2} c_1 \|\bar{\mathbf{w}}_+\|_2^2 + \frac{1}{2} c_2 \bar{\boldsymbol{\eta}}_-^\top \mathbf{U} \bar{\boldsymbol{\eta}}_- \\ & \leq \frac{1}{2} \mathbf{w}_+^\top \mathbf{Z}_+ \mathbf{Q} \mathbf{Z}_+^\top \mathbf{w}_+ + \frac{1}{2} c_1 \|\mathbf{w}_+\|_2^2 + \frac{1}{2} c_2 \boldsymbol{\eta}_-^\top \mathbf{U} \boldsymbol{\eta}_-. \end{aligned} \quad (49)$$

Next, rewriting Eqs. (49) in component form, we can obtain the following inequality

$$\begin{aligned} & \sum_{i=1}^{m_+} \frac{(\mathbf{z}_i^{+\top} \bar{\mathbf{w}}_+)^T \mathbf{z}_i^{+\top} \bar{\mathbf{w}}_+}{2|\mathbf{w}_+^\top \mathbf{z}_i^+|} + \frac{1}{2} c_1 \|\bar{\mathbf{w}}_+\|_2^2 + \frac{1}{2} c_2 \sum_{j=1}^{m_-} \frac{(\bar{\eta}_j^-)^2}{|\eta_j^-|} \\ & \leq \sum_{i=1}^{m_+} \frac{(\mathbf{z}_i^{+\top} \mathbf{w}_+)^T \mathbf{z}_i^{+\top} \mathbf{w}_+}{2|\mathbf{w}_+^\top \mathbf{z}_i^+|} + \frac{1}{2} c_1 \|\mathbf{w}_+\|_2^2 + \frac{1}{2} c_2 \sum_{j=1}^{m_-} \frac{(\eta_j^-)^2}{|\eta_j^-|}. \end{aligned} \quad (50)$$

Furthermore, let $\sqrt{x} = |\mathbf{z}_i^{+\top} \bar{\mathbf{w}}_+|$, $\sqrt{y} = |\mathbf{z}_i^{+\top} \mathbf{w}_+|$, $\sqrt{z} = |\bar{\eta}_j^-|$, $\sqrt{t} = |\eta_j^-|$, $c = c_2$. From Lemma 2, we have the following inequality

$$\begin{aligned} & |\mathbf{z}_i^{+\top} \bar{\mathbf{w}}_+| - \frac{(\mathbf{z}_i^{+\top} \bar{\mathbf{w}}_+)^T (\mathbf{z}_i^{+\top} \bar{\mathbf{w}}_+)}{2|\mathbf{z}_i^{+\top} \mathbf{w}_+|} + c_2 \left(|\bar{\eta}_j^-| - \frac{(\bar{\eta}_j^-)^2}{|\eta_j^-|} \right) \\ & \leq |\mathbf{z}_i^{+\top} \mathbf{w}_+| - \frac{(\mathbf{z}_i^{+\top} \mathbf{w}_+)^T (\mathbf{z}_i^{+\top} \mathbf{w}_+)}{2|\mathbf{z}_i^{+\top} \mathbf{w}_+|} + c_2 \left(|\eta_j^-| - \frac{(\eta_j^-)^2}{|\eta_j^-|} \right). \end{aligned} \quad (51)$$

Thus based on Eq. (51), we can further obtain the following inequality

$$\begin{aligned} & \sum_{i=1}^{m_+} |\mathbf{z}_i^{+\top} \bar{\mathbf{w}}_+| - \sum_{i=1}^{m_+} \frac{(\mathbf{z}_i^{+\top} \bar{\mathbf{w}}_+)^T (\mathbf{z}_i^{+\top} \bar{\mathbf{w}}_+)}{2|\mathbf{z}_i^{+\top} \mathbf{w}_+|} + c_2 \sum_{j=1}^{m_-} |\bar{\eta}_j^-| - c_2 \sum_{j=1}^{m_-} \frac{(\bar{\eta}_j^-)^2}{|\eta_j^-|} \\ & \leq \sum_{i=1}^{m_+} |\mathbf{z}_i^{+\top} \mathbf{w}_+| - \sum_{i=1}^{m_+} \frac{(\mathbf{z}_i^{+\top} \mathbf{w}_+)^T (\mathbf{z}_i^{+\top} \mathbf{w}_+)}{2|\mathbf{z}_i^{+\top} \mathbf{w}_+|} + c_2 \sum_{j=1}^{m_-} |\eta_j^-| - c_2 \sum_{j=1}^{m_-} \frac{(\eta_j^-)^2}{|\eta_j^-|}. \end{aligned} \quad (52)$$

Then further combining Eqs. (50) and (52), we have

$$\begin{aligned} & \sum_{i=1}^{m_+} |\mathbf{z}_i^{+\top} \bar{\mathbf{w}}_+| + \frac{1}{2} c_1 \|\bar{\mathbf{w}}_+\|_2^2 + c_2 \sum_{j=1}^{m_-} |\bar{\eta}_j^-| \\ & \leq \sum_{i=1}^{m_+} |\mathbf{z}_i^{+\top} \mathbf{w}_+| + \frac{1}{2} c_1 \|\mathbf{w}_+\|_2^2 + c_2 \sum_{j=1}^{m_-} |\eta_j^-|. \end{aligned} \quad (53)$$

Thus we can obtain the following inequality

$$\begin{aligned} & \sum_{i=1}^{m_+} \min \left(|\mathbf{z}_i^{+\top} \bar{\mathbf{w}}_+|, \varepsilon \right) + \frac{1}{2} c_1 \|\bar{\mathbf{w}}_+\|_2^2 + c_2 \sum_{j=1}^{m_-} \min \left(|\bar{\eta}_j^-|, \varepsilon \right) \\ & \leq \sum_{i=1}^{m_+} \min \left(|\mathbf{z}_i^{+\top} \mathbf{w}_+|, \varepsilon \right) + \frac{1}{2} c_1 \|\mathbf{w}_+\|_2^2 + c_2 \sum_{j=1}^{m_-} \min \left(|\eta_j^-|, \varepsilon \right). \end{aligned} \quad (54)$$

□

Thus we have $J(\bar{\mathbf{w}}_+, \bar{\boldsymbol{\eta}}_-) \leq J(\mathbf{w}_+, \boldsymbol{\eta}_-)$ established. Similarly, when $\mathbf{z}_i^{+\top} \mathbf{w}_+ > \varepsilon$ and $\eta_j^- > \varepsilon$ are satisfied, we have $J(\bar{\mathbf{w}}_+, \bar{\boldsymbol{\eta}}_-) = J(\mathbf{w}_+, \boldsymbol{\eta}_-)$. In summary, $J(\bar{\mathbf{w}}_+, \bar{\boldsymbol{\eta}}_-) \leq J(\mathbf{w}_+, \boldsymbol{\eta}_-)$ holds. This means that Algorithm 1 will decrease the objective function of the optimization problem (15) until it converges. The proof process is similar for the optimization problem (16).

Theorem 2. *Algorithm 1 will converge to a local optimum to the optimization problem (20).*

Proof. Here we use optimization problem (20) as an example to prove the Theorem 2. When $|\mathbf{w}_+^\top \mathbf{z}_i^+| < \varepsilon$ and $|\eta_j^-| < \varepsilon$, the Lagrangian function of the optimization problem (20) is given as follows

$$\begin{aligned} L_1(\mathbf{w}_+, \boldsymbol{\eta}_-, \boldsymbol{\alpha}) = & \sum_{i=1}^{m_+} |\mathbf{w}_+^\top \mathbf{z}_i^+| + \frac{1}{2} c_1 \|\mathbf{w}_+\|_2^2 + c_2 \sum_{j=1}^{m_-} |\eta_j^-| \\ & - \boldsymbol{\alpha}^\top (-\mathbf{Z}_-^\top \mathbf{w}_+ + \boldsymbol{\eta}_- - \mathbf{e}_-). \end{aligned} \quad (55)$$

Then to obtain the gradient of $L_1(\mathbf{w}_+, \boldsymbol{\eta}_-, \boldsymbol{\alpha})$ with respect to \mathbf{w}_+ , we have

$$\begin{aligned} \frac{\partial L_1(\mathbf{w}_+, \boldsymbol{\eta}_-, \boldsymbol{\alpha})}{\partial \mathbf{w}_+} = & \sum_{i=1}^{m_+} \frac{\mathbf{z}_i^+ \mathbf{z}_i^{+\top} \mathbf{w}_+}{|\mathbf{w}_+^\top \mathbf{z}_i^+|} + c_1 \mathbf{I} \mathbf{w}_+ + \mathbf{Z}_- \boldsymbol{\alpha} \\ = & \mathbf{Z}_+ \mathbf{Q} \mathbf{Z}_+^\top \mathbf{w}_+ + c_1 \mathbf{I} \mathbf{w}_+ + \mathbf{Z}_- \boldsymbol{\alpha} = \mathbf{0}. \end{aligned} \quad (56)$$

Similarly, we can obtain the Lagrangian function of the optimization problem (22) as follows

$$L_2(\mathbf{w}_+, \boldsymbol{\eta}_-, \boldsymbol{\alpha}) = \frac{1}{2} (\mathbf{Z}_+^\top \mathbf{w}_+)^T \mathbf{Q} \mathbf{Z}_+^\top \mathbf{w}_+ + \frac{1}{2} c_1 \|\mathbf{w}_+\|_2^2 + \frac{1}{2} c_2 \boldsymbol{\eta}_-^\top \mathbf{U} \boldsymbol{\eta}_- - \boldsymbol{\alpha}^\top (-\mathbf{Z}_-^\top \mathbf{w}_+ + \boldsymbol{\eta}_- - \mathbf{e}_-). \quad (57)$$

Then the gradient of $L_2(\mathbf{w}_+, \boldsymbol{\eta}_-, \boldsymbol{\alpha})$ with respect to \mathbf{w}_+ yields

$$\frac{\partial L_2(\mathbf{w}_+, \boldsymbol{\eta}_-, \boldsymbol{\alpha})}{\partial \mathbf{w}_+} \Rightarrow \mathbf{Z}_+ \mathbf{Q} \mathbf{Z}_+^\top \mathbf{w}_+ + c_1 \mathbf{I} \mathbf{w}_+ + \mathbf{Z}_- \boldsymbol{\alpha} = \mathbf{0}. \quad (58)$$

□

It is easy to observe that Eqs. (56) and (58) are equivalent when Algorithm 1 converges, which satisfies the Lagrangian function condition of the optimization problem (20). Thus we can solve the optimization problem (22) instead of the optimization problem (20). This means that the convergent solution satisfies Eq. (58) when it is a locally optimal solution of the optimization problem (20). A similar proof is available for problem (21).

3.3. Time complexity

In this subsection, we briefly analyze the time complexity of Algorithm 1 for the optimization problem (15). Let m_+ and m_- be the number of positive and negative samples, respectively. n represents the feature number of the samples and let $m_l = \frac{n^2+3n+2}{2}$. And T represents the maximum number of iterations, it should be noted that $T = 30$ in our experiments. The time complexity of Algorithm 1 is mainly in the matrix inverse operation, thus we need to analyze its time complexity in the following two cases. When $m_l \geq m_-$, the time complexity of Algorithm 1 is $O(Tm_-^3)$. When $m_l < m_-$, the time complexity of Algorithm 1 is $O(Tm_l^3)$. Thus, the time complexity of Algorithm 1 for the optimization problem (15) is $O(T\min(m_l^3, m_-^3))$. In summary, our CL₁QTSVM model requires time complexity of $O(T(\min(m_l^3, m_-^3) + \min(m_l^3, m_+^3)))$.

3.4. Comparison methods

To better distinguish it from the comparative state-of-the-art methods, our model is compared with the above methods, as shown in Table 1. As a result, it can be summarized that our method has the following four major advantages. (1) Our model uses the Capped L_1 -norm distance metric,

which results in its insensitivity to outliers. (2) Our model does not involve the selection of kernel function and kernel parameters, and has stronger interpretability. (3) The introduction of the L_2 regularization term leads our method to follow the structural risk minimization (SRM) principle, and further improves the generalization ability of our model. (4) An efficient iterative algorithm is used to solve the optimization model, resulting in low time cost.

Table 1: Comparison between different methods.

Model	Loss function	Distance norm	L_2 regularization term	Kernel function	Time complexity
TSVM (Chandra and Khemchandani, 2007)	Hinge loss	L_2 -norm	No	Yes	$O\left(\frac{m^3}{4} + (m+1)^3\right)$
CL_1 -FRTBSVM (Ma et al., 2020)	Capped L_1 -norm	Capped L_1 -norm	Yes	Yes	$O(2T(m+1)^3)$
CL_1 -FRTELM (Ma, 2020)	Capped L_1 -norm	Capped L_1 -norm	No	No	$O(2(L^3 + n^3))$
LINEX-TSVM (Wang et al., 2022)	Capped LINEX loss	Capped L_1 -norm	Yes	Yes	$O(T(\frac{m^3}{4} + (n+1)^3))$
$CL_{2,p}$ -LSTSVM (Yuan and Yang, 2021)	Square loss	Capped $L_{2,p}$ -norm	No	Yes	$O(T(m \times (n+1)^2 + (n+1)^3))$
ν -FRSQSSVM (Gao et al., 2022)	Fuzzy hinge loss	Fuzzy L_2 -norm	No	No	$O(m^3 + (2n+1)^3)$
LSQTSVM (Gao et al., 2019)	Square loss	L_2 -norm	No	No	$O(\frac{n^2+3n+2}{2} \times \frac{n^2+3n+2}{2})$
CL_1 QTSVM	Capped L_1 -norm	Capped L_1 -norm	Yes	No	$O(T(\min(m_1^3, m_2^3) + \min(m_1^3, m_2^3)))$

4. Numerical experiments

In this section, we first perform experiments on synthetic dataset, benchmark dataset and image dataset, and compare our method with the rest seven state-of-the-art methods. Then, parametric sensitivity analysis, convergence analysis and nonparametric tests are also performed to verify the effectiveness of our method.

4.1. Experiment setups

- (1) Running environment. All experiments were run on a 16GB RAM and Inter Core i7-4790 desktop computer.
- (2) Benchmark dataset description.

- In the synthetic numerical experiments, we use three synthetic datasets, Example 1, Example 2 and Example 3, as shown in Figure ???. To further compare the classification performance of each method under different label noise ratios, we add 5% and 10% label noise to Example 1, Example 2 and Example 3 respectively.
- In the numerical experiments on real data, we first use 16 benchmark datasets, which are all from the UCI database, and the details of these 16 benchmark datasets are listed in Table 2. In addition, image datasets are also used, and their details are described in the following subsections.

Table 2: Description of the benchmark datasets.

Dataset	#Instances	#Attributes
Australian	690	14
Indian	583	10
Blood	748	4
Cleve	296	13
Climate-simulation	540	18
CMC	1473	9
Cylinder-bands	512	35
Glass(0-1-5 vs. 2)	192	9
Haberman	306	3
Hepatitis	155	19
Ionosphere	351	32
Sonar	208	60
Vote	435	16
WBC	683	9
Yeast(2 vs. 8)	264	8
Robotnavig	2923	24

(3) Data preprocessing. Before the experiment, all data are normalized to $[-1, 1]$.

(4) Parameter setting. In all numerical experiments, the 5-fold cross-validation method and grid search method were used to select the optimal parameters for each model. The final classification result is the average of 10 times 10-fold cross-validation. For the nonlinear case, the Gaussian kernel $\mathcal{K}(\mathbf{u}, \mathbf{v}) = \exp\left(-\frac{\|\mathbf{u}-\mathbf{v}\|^2}{2\sigma^2}\right)$ is used, the kernel parameter σ is chosen from the set $\{2^i|i = -5, -4, \dots, 4, 5\}$. The loss function regularization parameter c_2 and the regularization parameter c_1 of all methods are selected from the set $\{10^i|i = -5, -4, \dots, 4, 5\}$. In addition, the specific parameter selection details of some comparison methods are as follows

- For FRTEL M model (Ma, 2020), hidden layer node parameter $L \in \{20, 40, 50, 100, 200\}$.
- For the LINEX-TSVM model (Wang et al., 2022), Capped LINEX loss function parameter $a = 1$, convergence precision is set to $\epsilon = 10^{-4}$.
- For $CL_{2,p}$ LSTSVM model (Yuan and Yang, 2021), the truncation parameter ϵ is selected from the set $\{10^i|i = -5, -3, \dots, 3, 5\}$, with parameters p selected from the set $\{1.1, 1.3, \dots, 1.9\}$, the convergence accuracy is set to $\epsilon = 10^{-4}$.
- For ν -FRSQSSVM model (Gao et al., 2022), the parameters ν is chosen from the set $\{0.05, 0.1, \dots, 0.9, 0.99\}$.

(5) Evaluation metrics . The experimental part of this section uses Accuracy (Acc) and F1 Score (F1) to evaluate the classification performance of

each method, which are defined as follows

$$\text{Acc} = \frac{TP + TN}{TP + FN + TN + FP}, \quad (59)$$

$$\text{F1} = \frac{2TP}{2TP + FN + FP}, \quad (60)$$

where TN and TP represent the number of correctly predicted positive and negative samples, respectively. And FP and FN represent the number of incorrectly predicted positive and negative samples, respectively. In addition, the standard deviation of the test accuracy (Std) is also used.

4.2. Experiments results

In this subsection, we focus on comparing the classification performance of our method with the rest of the state-of-the-art methods on synthetic datasets, benchmark datasets, and image datasets.

4.2.1. Performance on synthetic dataset

First, we compare the classification performance of the CL_1 QTSVM model with other state-of-the-art methods on three synthetic datasets. The construction methods and images of the three synthetic datasets are shown as follows:

Example 1:

class +1: $[x_i]_2 = 0.2222[x_i]_1^2 + 0.5 + \xi_i, [x_i]_1 \sim U[-3, 3]$,
 class -1: $[x_j]_2 = -0.2222[x_j]_1^2 + 1.5 + \xi_j, [x_j]_1 \sim U[-3, 3]$,
 where $\xi_i, \xi_j \sim N(0, 0.1), i, j = 1, 2, \dots, 200$.

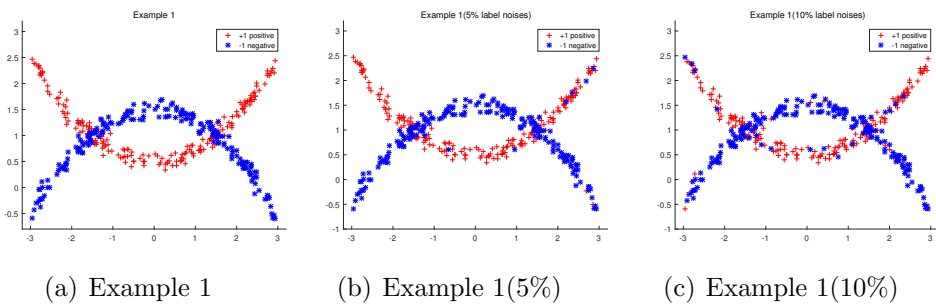


Figure 2: The distribution of data for Example 1 with different label noise ratios.

Example 2:

class +1: $[x_i]_1 = 3\cos(\theta_i)$, $[x_i]_2 = 3\sin(\theta_i) + \xi_i$, $\theta_i \sim U[0, 2\pi]$,

class -1: $[x_j]_1 = 3\cos(\theta_j)$, $[x_j]_2 = 3\sin(\theta_j) + \xi_j$, $\theta_j \sim U[\pi, 2\pi]$,

where $\xi_i, \xi_j \sim N(0, 0.2)$, $i, j = 1, 2, \dots, 200$.

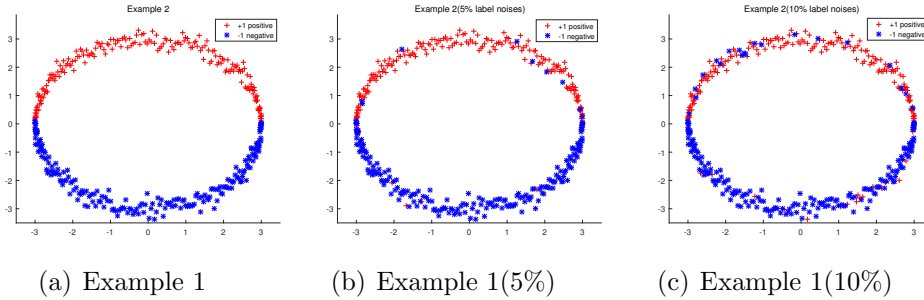


Figure 3: The distribution of data for Example 2 with different label noise ratios.

Example 3:

class +1: $[x_i]_2 = 0.75[x_i]_1^2 + 1.5[x_i]_1 + 0.75 + \xi_i$, $[x_i]_1 \sim U[-3, 1]$,

class -1: $[x_j]_2 = 0.75[x_j]_1^2 - 1.5[x_j]_1 + 0.75 + \xi_j$, $[x_j]_1 \sim U[-1, 3]$,

where $\xi_i, \xi_j \sim N(0, 0.1)$, $i, j = 1, 2, \dots, 200$.

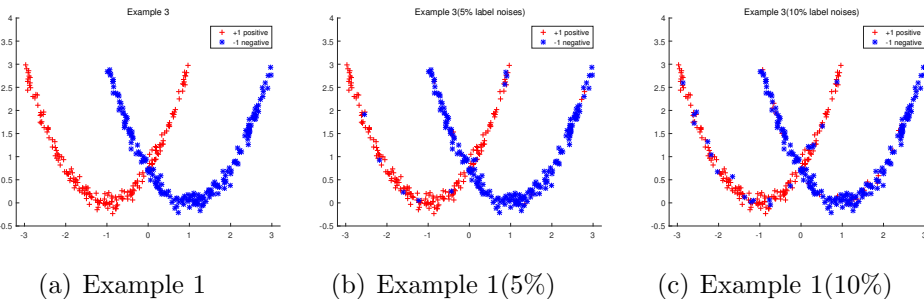


Figure 4: The distribution of data for Example 3 with different label noise ratios.

The classification results on the synthetic datasets as well as on the synthetic datasets with different percentages of labeled noises are shown in Table 3. It should be noted that for the FRTELM method, the activation function is $\frac{1}{1+exp(-(\mathbf{w}^\top \mathbf{x} + b))}$, where \mathbf{w} and b are randomly generated. From the classification results in Table 3, it can be seen that on the synthetic datasets Example 1, Example 2 and Example 3 without label noises, the classification accuracies of our CL_1 QTSVM model are not the highest, but second

to the optimal method. However, our CL_1 QTSVM model has the highest classification accuracy on the synthetic datasets Example 1, Example 2 and Example 3 with label noises. Specifically, on the dataset Example 1 with 5% and 10% label noises, the classification accuracies of our CL_1 QTSVM model are higher than the second ranked method by 0.71% and 1.83%, respectively. And on the dataset Example 2 with 5% and 10% label noises, the classification accuracies of our CL_1 QTSVM model are higher than the second ranked method by 0.15% and 0.08%, respectively. And on the dataset Example 3 with 5% and 10% label noises, the classification accuracy of our CL_1 QTSVM model is higher than the second-ranked method by 0.62% and 1.80%, respectively. These results validate the advantage of our method in handling data with label noises, which also prepare the way for the experiments of our CL_1 QTSVM model on real datasets.

Table 3: Experimental results on synthetic datasets.

Datasets	TSVM (Acc,Std)(%) (c_1, c_2, σ)	CL_1 FRTBSVM (Acc,Std)(%) (c_1, c_2, σ)	CL_1 FRTELM (Acc,Std)(%) (c_2, L)	LINEX-TSVM (Acc,Std)(%)	$CL_{2,p}$ -LSTSVM (Acc,Std)(%) (c_1, c_2, ϵ, p)	ν -FRSQSSVM (Acc,Std)(%) (c_2)	LSQTSVM (Acc,Std)(%) (c_1, c_2)	CL_1 QTSVM (Acc,Std)(%) (c_1, c_2)
Example 1	(91.75,1.13) ($10^{-5}, 2^{-1}$)	(94.45,0.16) ($10^3, 10^{-5}, 2^5$)	(91.53,1.00) ($10^{-3}, 20$)	(53.88,0.39) ($10^2, 10^{-4}$)	(62.86,0.56) ($10^{-5}, 10^{-5}, 1.7$)	(50.40,1.10) (0.01)	(93.95,0.31) (10^{-1})	(94.03,0.38) ($10^2, 10^1$)
Example 1(5%)	(86.77,0.77) ($10^{-5}, 2^{-3}$)	(85.88,0.82) ($10^3, 10^{-5}, 2^9$)	(83.60,1.37) ($10^5, 10^{-5}, 2^0$)	(51.96,0.91) ($10^{-5}, 200$)	(59.36,0.34) ($10^{-3}, 10^1$)	(50.52,1.12) (0.01)	(83.25,0.50) (10^0)	(87.48,0.36) ($10^{-1}, 10^2$)
Example 1(10%)	(80.88,1.17) ($10^{-5}, 2^{-3}$)	(80.92,1.21) ($10^5, 10^5, 2^0$)	(77.10,1.89) ($10^{-5}, 500$)	(53.27,2.39) ($10^{-2}, 10^{-4}$)	(59.92,0.58) ($10^{-3}, 10^{-1}, 1.7$)	(46.50,1.92) (0.4)	(64.20,1.12) (10^0)	(82.75,0.24) ($10^0, 10^4$)
Example 2	(98.50,0.20) ($10^{-5}, 2^{-3}$)	(98.05,0.42) ($10^1, 10^{-1}, 2^3$)	(97.55,0.63) ($10^{-3}, 100$)	(89.02,0.57) ($10^{-4}, 10^{-1}$)	(98.07,0.16) ($10^3, 10^3, 1.5$)	(97.75,0.61) (0.2)	(97.77,0.18) (10^{-2})	(98.17,0.26) ($10^0, 10^2$)
Example 2(5%)	(93.42,0.61) ($10^{-3}, 2^{-1}$)	(93.35,0.21) ($10^{-1}, 10^{-1}, 2^0$)	(92.85,1.74) ($10^{-1}, 40$)	(85.56,0.54) ($10^{-4}, 10^1$)	(93.52,0.29) ($10^1, 10^3, 1.3$)	(93.32,0.29) (0.4)	(89.75,1.03) (10^3)	(93.67,0.29) ($10^{-3}, 10^{-5}$)
Example 2(10%)	(87.35,1.25) ($10^{-5}, 2^{-1}$)	(87.92,0.42) ($10^{-1}, 10^{-5}, 2^0$)	(85.82,0.88) ($10^{-5}, 500$)	(78.90,0.42) ($10^0, 10^3$)	(87.20,0.25) ($10^{-3}, 10^3, 1.3$)	(86.95,0.39) (0.4)	(82.70,0.39) (10^{-5})	(88.00,1.60) ($10^{-2}, 10^{-1}$)
Example 3	(98.50,0.42) ($10^{-5}, 2^{-3}$)	(98.63,0.56) ($10^{-3}, 10^{-1}, 2^0$)	(98.07,0.64) ($10^5, 500$)	(86.19,0.29) ($10^0, 10^{-3}$)	(82.47,0.14) ($10^{-3}, 10^3, 1.5$)	(74.42,0.70) (0.01)	(98.95,0.11) (10^{-5})	(98.83,0.12) ($10^{-5}, 10^{-4}$)
Example 3(5%)	(91.78,0.59) ($10^{-5}, 2^{-2}$)	(92.30,0.39) ($10^0, 10^{-3}, 2^0$)	(90.50,0.74) ($10^{-5}, 500$)	(82.24,0.55) ($10^{-2}, 10^{-5}$)	(79.07,0.88) ($10^{-5}, 10^{-1}, 1.5$)	(74.72,0.55) (0.2)	(87.78,1.11) (10^0)	(92.92,1.81) ($10^{-3}, 10^0$)
Example 3(10%)	(86.20,1.02) ($10^{-4}, 2^{-1}$)	(86.15,0.46) ($10^{-1}, 10^{-5}, 2^0$)	(84.38,1.63) ($10^{-1}, 20$)	(76.83,0.70) ($10^{-1}, 10^{-4}$)	(75.86,0.41) ($10^{-5}, 10^3, 1.5$)	(70.42,0.54) (0.4)	(77.03,0.85) (10^2)	(88.00,1.60) ($10^{-1}, 10^3$)

4.2.2. Performance on benchmark datasets

Table 4 shows the classification results of our CL_1 QTSVM model with the rest of the compared methods on the 16 benchmark datasets, where the optimal results are shown in bold. In addition, for the FRTELM method, the activation function is $\frac{1}{1+exp(-(\mathbf{w}^\top \mathbf{x} + b))}$, where \mathbf{w} and b are randomly generated. From the experimental results on the 16 benchmark datasets without noise in Table 4, it can be seen that the classification accuracies of our CL_1 QTSVM model are the highest on 8 of the datasets. Specifically, on the benchmark datasets Ionosphere, Sonar, Vote, WBC, Yeast (2 vs. 8), and Robotnavig, our CL_1 QTSVM model outperforms the second-ranked method by 0.17%, 0.62%, 0.20%, and 0.04%, 0.13% and 0.03%, respectively; Also,

although our CL_1 QTTSVM model does not have the highest accuracy on the datasets Indian, Blood, and Glass (0-1-5 vs. 2), it is only lower than the classification accuracy of the best method on these three datasets by 0.67%, 0.40%, and 0.20%, respectively. These results demonstrate the effectiveness of our method.

Table 4: Experimental results on the benchmark dataset.

Datasets	TSVM (Acc,Std)(%) (c_2, σ)	CL_1 FRTBSVM (c_1, c_2, σ)	CL_1 FRTEL M (c_2, L)	LINEX-TSVM (c_1, c_2)	$CL_{2,p}$ -LSTSVM (c_2, ϵ, p)	ν -FRSQSSVM (c_2, ϵ, p)	LSQTSVM (c_2)	CL_1 QTTSVM (c_1, c_2)
Australian	(81.25,0.28) ($10^{-5}, 2^{-1}$)	(86.46,0.50) ($10^3, 10^{-3}, 2^4$)	(85.87,0.60) ($10^1, 50$)	(85.43,0.19) ($10^1, 10^4$)	(86.57,0.17) ($10^1, 10^5, 1.5$)	(86.65,0.21) (0.01)	(80.81,1.52) (10^{-2})	(86.66,0.32) ($10^{-3}, 10^{-5}$)
Indian	(71.33,0.19) ($10^1, 2^{-4}$)	(71.77,0.88) ($10^{-3}, 10^{-3}, 2^0$)	(70.11,1.04) ($10^{-5}, 500$)	(71.30,0.13) ($10^{-1}, 10^{-6}$)	(72.71,1.03) ($10^{-3}, 10^{-1}, 1.3$)	(69.72,0.80) (0.01)	(49.95,0.68) (10^{-4})	(72.04,0.52) ($10^{-3}, 10^0$)
Blood	(44.17,6.70) ($10^3, 2^{-1}$)	(78.20,0.40) ($10^{-5}, 10^{-5}, 2^0$)	(78.92,0.51) ($10^4, 200$)	(76.83,0.34) ($10^2, 10^{-2}$)	(77.33,0.08) ($10^{-1}, 10^5, 1.5$)	(78.64,0.68) (0.2)	(61.35,1.34) (10^{-4})	(78.24,0.12) ($10^{-5}, 10^0$)
Cleve	(75.98,2.85) ($10^3, 2^1$)	(81.06,0.97) ($10^1, 10^{-5}, 2^0$)	(78.49,1.83) ($10^{-5}, 20$)	(81.66,0.51) ($10^{-5}, 10^4$)	(82.19,0.69) ($10^{-3}, 10^3, 1.3$)	(83.44,0.18) (0.01)	(67.28,2.17) (10^{-1})	(81.07,1.52) ($10^{-3}, 10^{-2}$)
Climate-simulation	(93.72,0.42) ($10^{-5}, 2^1$)	(92.74,0.23) ($10^4, 10^{-5}, 2^0$)	(95.22,0.51) ($10^1, 200$)	(85.60,0.69) ($10^{-2}, 10^{-4}$)	(95.01,0.50) ($10^{-1}, 10^3, 1.5$)	(94.44,0.41) (0.01)	(93.20,0.59) (10^0)	(92.94,0.53) ($10^{-4}, 10^{-4}$)
CMC	(58.72,1.29) ($10^3, 2^{-1}$)	(70.47,0.46) ($10^3, 10^{-5}, 2^3$)	(68.10,0.55) ($10^2, 50$)	(68.39,0.17) ($10^3, 10^3$)	(67.55,0.22) ($10^{-3}, 10^3, 1.9$)	(67.94,0.61) (0.01)	(69.61,0.34) (10^{-4})	(70.67,0.40) ($10^{-5}, 10^0$)
Cylinder-bands	(72.18,1.34) ($10^{-5}, 2^{-3}$)	(68.40,3.92) ($10^{-3}, 10^3, 2^0$)	(68.77,2.63) ($10^{-5}, 50$)	(67.94,0.75) ($10^{-5}, 10^5$)	(70.18,0.64) ($10^{-1}, 10^1, 1.5$)	(73.81,0.76) (0.01)	(69.18,1.44) (10^0)	(72.99,1.74) ($10^{-3}, 10^0$)
Glass(0-1-5 vs. 2)	(91.13,0.05) ($10^{-5}, 2^{-2}$)	(90.91,0.79) ($10^3, 10^{-1}, 2^0$)	(78.88,9.25) ($10^1, 100$)	(58.12,0.11) ($10^{-4}, 10^1$)	(90.16,0.34) ($10^{-5}, 10^{-5}, 1.9$)	(91.13,0.04) (0.8)	(73.82,2.26) (10^{-1})	(90.93,0.28) ($10^{-3}, 10^2$)
Haberman	(59.12,4.02) ($10^{-3}, 2^{-1}$)	(74.48,0.95) ($10^5, 10^{-3}, 2^3$)	(70.96,2.15) ($10^1, 50$)	(75.46,0.41) ($10^{-2}, 10^5$)	(76.17,0.53) ($10^{-3}, 10^3, 1.5$)	(74.23,0.97) (0.01)	(71.30,0.83) (10^4)	(74.93,0.35) ($10^{-3}, 10^0$)
Hepatitis	(81.00,1.22) ($10^3, 2^1$)	(80.66,1.62) ($10^3, 10^{-5}, 2^3$)	(80.43,1.58) ($10^1, 20$)	(76.77,0.81) ($10^{-3}, 10^3$)	(82.10,1.15) ($10^{-3}, 10^3, 1.9$)	(84.91,1.32) (0.01)	(73.41,2.37) (10^{-2})	(83.38,1.48) ($10^4, 10^5$)
Ionosphere	(89.81,0.79) ($10^5, 2^1$)	(90.23,0.62) ($10^1, 10^{-5}, 2^3$)	(89.83,0.57) ($10^1, 20$)	(89.06,0.46) ($10^{-2}, 10^3$)	(88.67,0.30) ($10^{-1}, 10^{-3}, 1.7$)	(89.92,0.43) (0.01)	(88.69,0.87) (10^{-5})	(90.40,0.69) ($10^1, 10^4$)
Sonar	(83.99,1.65) ($10^{-2}, 2^2$)	(83.22,1.29) ($10^3, 10^{-3}, 2^3$)	(55.67,3.34) ($10^{-2}, 40$)	(73.12,1.07) ($10^0, 10^3$)	(73.90,0.90) ($10^{-1}, 10^3, 1.3$)	(82.69,1.01) (0.2)	(86.40,1.49) (10^{-5})	(87.02,0.94) ($10^{-1}, 10^1$)
Vote	(94.46,0.54) ($10^{-5}, 2^1$)	(94.57,0.25) ($10^1, 10^{-5}, 2^2$)	(89.86,0.94) ($10^1, 20$)	(94.83,0.22) ($10^0, 10^4$)	(94.21,0.21) ($10^{-3}, 10^3, 1.7$)	(94.20,0.41) (0.01)	(90.32,0.93) (10^3)	(95.03,0.36) ($10^{-5}, 10^{-1}$)
WBC	(95.77,0.30) ($10^1, 2^{-1}$)	(97.09,0.24) ($10^1, 10^{-5}, 2^0$)	(93.63,1.75) ($10^1, 50$)	(95.96,0.43) ($10^{-3}, 10^4$)	(95.76,0.09) ($10^{-3}, 10^1, 1.9$)	(96.47,0.11) (0.01)	(76.10,0.62) (10^1)	(97.13,0.25) ($10^{-1}, 10^{-4}$)
Yeast(2 vs. 8)	(94.33,0.39) ($10^{-1}, 2^{-4}$)	(94.47,0.71) ($10^{-1}, 10^{-5}, 2^0$)	(92.32,4.59) ($10^4, 20$)	(95.21,0.65) ($10^{-2}, 10^{-2}$)	(95.16,0.21) ($10^{-5}, 10^3, 1.3$)	(95.20,0.17) (0.01)	(95.08,0.26) (10^{-3})	(95.34,0.26) ($10^{-3}, 10^{-5}$)
Robotnavig	(94.19,0.26) ($10^{-3}, 2^{-1}$)	(98.78,0.08) ($10^1, 10^{-5}, 2^3$)	(94.27,0.33) ($10^{-2}, 500$)	(80.78,0.32) ($10^2, 10^{-2}$)	(84.83,0.11) ($10^1, 10^1, 1.3$)	(88.17,1.46) (0.01)	(95.08,0.26) (10^{-2})	(98.81,0.09) ($10^{-5}, 10^{-1}$)

4.2.3. Performance on image datasets

Table 5 shows the basic information of the four image datasets used in this subsection. And some images from these four image datasets are shown in Figure 5(a)-(d). In particular, the USPS dataset and the COIL20 dataset are from the URL ¹, while the Yale dataset and the ORL dataset are from the URL ². For the USPS handwritten digit recognition datasets, we use 9298 images, in which each image has 16×16 pixels, and the label of each image belongs to one of the digits 0 to 9. For the COIL20 dataset, it contains 20 objects with 72 images each, and each image with a pixel size of 32×32 . Each

¹<http://www.cad.zju.edu.cn/home/dengcai/Data/MLData.html>

²<https://jundongl.github.io/scikit-feature/datasets.html>

object in this dataset has its images taken 5 degrees apart as it rotates on a turntable. For the Yale dataset, which consists of 165 grayscale images in GIF format of 15 individuals, there are 11 images for each subject, and each image has a different facial expression or composition, e.g., center light, glasses, happy, left light, no glasses, normal, right light, sad, sleepy, surprised, and blinking. And the pixel size of each image is 32×32 . For the ORL dataset, the dataset consists of 40 different subjects, each subject has 10 different photos. For some subjects, the images were taken at different times, with different lighting, facial expressions (eyes open/close, smiling/not smiling) and facial details (glasses/no glasses). All images were taken against a dark, uniform background, and subjects were held in an upright, frontal position (with some lateral movement allowed). In addition, each image in the ORL dataset has 32×32 pixels.

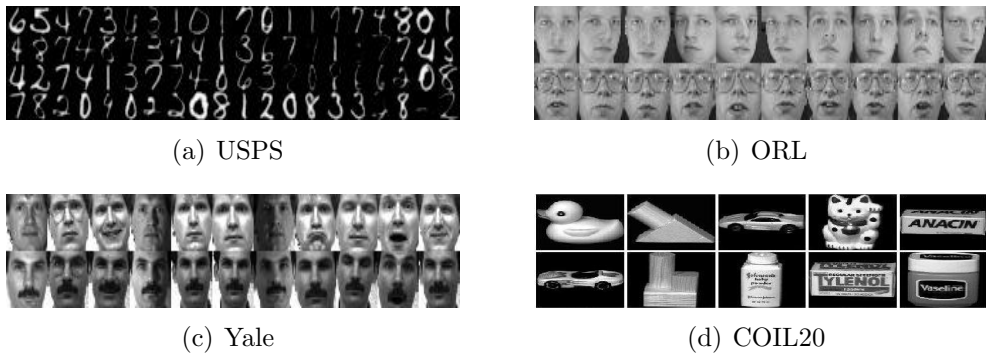


Figure 5: Visualization results for four image datasets.

Before we analyze the experimental results on the image dataset, one detail of the experiment needs to be explained. Since the feature dimensions of the image dataset are much higher than those of the benchmark datasets and the synthetic datasets, the time complexity of the CL_1 QTSVM and LSQTSVM models grows quadratically with the feature dimensions. In order to reduce the time complexity and computational memory, in this paper, both the CL_1 QTSVM model and LSQTSVM model are simplified using the diagonal vectorization operator and the reduced quadratic vectorization operator without cross terms (Gao et al., 2022), then the equations (17)-(19) are rewritten as

$$\boldsymbol{\omega}_+ \triangleq [\text{dvec}^\top(\mathbf{W}_+), \mathbf{b}_+^\top, c_+]^\top \in \mathbb{R}^{2n+1}, \quad (61)$$

$$\boldsymbol{\omega}_- \triangleq [\text{dvec}^\top(\mathbf{W}_-), \mathbf{b}_-^\top, c_+]^\top \in \mathbb{R}^{2n+1}, \quad (62)$$

$$\mathbf{h}_j^- \triangleq [\text{qvec}^\top(\mathbf{x}_j), \mathbf{x}_j^\top, 1]^\top \in \mathbb{R}^{2n+1}, j = 1, 2, \dots, m_-, \quad (63)$$

$$\mathbf{h}_i^+ \triangleq [\text{qvec}^\top(\mathbf{x}_i), \mathbf{x}_i^\top, 1]^\top, i = 1, 2, \dots, m_+. \quad (64)$$

Therefore, based on the Eqs. (61)-(64), the time complexity of the CL_1 QTSVM model and the LSQTSVM model on the image datasets is greatly decreased.

The data are normalized to $[-1, 1]$ before performing the experiments. Both the CL_1 FRTBSVM model and the TSVM model use the RBF kernel function. The evaluation metrics used are Acc and F1, which are obtained by the average of 10 times 10-fold cross-validation. Time is the sum of the training time and testing time of a 10-fold cross validation. Table 6 and Table 7 show the classification results and optimal parameters of the CL_1 QTSVM model and the rest of the compared state-of-the-art methods on the four image datasets. As shown in Table 6, the classification accuracy of our CL_1 QTSVM model on Yale dataset, USPS dataset and ORL dataset are the optimal results, which are higher than the second ranked method by 1.94%, 0.01% and 0.05% respectively. The CL_1 QTSVM model is not the optimal result on the COIL20 dataset, but its classification accuracy is only 0.45% lower than that of the CL_1 FRTBSVM model. Similarly, from Table 7, it can also be seen that the F1 scores of CL_1 QTSVM model on the Yale dataset, USPS dataset, and ORL dataset are the optimal results, which are higher than the second-ranked method by 2.37%, 0.62%, and 0.08%, respectively. The CL_1 QTSVM model is not the optimal result on the COIL20 dataset, but its classification accuracy is only 0.35% lower than that of the CL_1 FRTBSVM model.

Table 8 briefly shows the running time of each method on the four image datasets, where the running time is the sum of the testing time and training time. From the results shown in Table 8, the following conclusions about our CL_1 QTSVM model can be obtained: (1) The running time of the CL_1 QTSVM model on the USPS dataset is much lower than that of the TSVM, CL_1 FRTBSVM, and ν -FRSQSSVM models, which is mainly due to the fact that our model uses the SMW theorem and the reduced quadratic quantization operator without cross-terms. (2) On the COIL20, USPS and ORL datasets, the running time of the CL_1 QTSVM model is not as good as that of the CL_1 FRTBSVM, the CL_1 FRTEL and the LINEX-TSVM, but it is not much different from them. (3) As shown from the average running time

results, the running time of the CL_1 QTSVM model is not only much lower than that of TSVM, CL_1 FRTEL, ν -FRSQSSVM and $CL_{2,p}$ -LSTSVM, but also comparable to that of CL_1 FRTEL, LINEX-TSVM and LSQTSVM. .

Table 5: Basic information on four image recognition datasets.

Dataset	Classification	#Instances	#Attributes
COIL20	(0~10,11~20)	1440	1024
USPS	(0~4,5~9)	9298	256
Yale	(1~7,8~15)	165	1024
ORL	(1~5,6~10)	100	1024

Table 6: Optimal accuracy and optimal parameter results for each method on four image datasets.

Datasets	TSVM (Acc,Std)(%) (c_2, σ)	CL_1 FRTEB SVM (Acc,Std)(%) (c_1, c_2, σ)	CL_1 FRTEL M (Acc,Std)(%) (c_2, L)	LINEX-TSVM (Acc,Std)(%) (c_1, c_2)	$CL_{2,p}$ -LSTSVM (Acc,Std)(%) (c_2, ϵ, p)	ν -FRSQSSVM (Acc,Std)(%) (ν)	LSQTSVM (Acc,Std)(%) (c_2)	CL_1 QTSVM (Acc,Std)(%) (c_1, c_2)
COIL20	(99.72,0.13) ($10^5, 2^3$)	(100.00,0.00) ($10^1, 10^{-5}, 2^3$)	(52.23,1.98) ($10^1, 50$)	(94.66,0.12) ($10^{-1}, 10^5$)	(95.89,0.15) ($10^{-3}, 10^3, 1.9$)	(95.80,0.37) (0.01)	(96.98,0.19) (10^2)	(99.55,0.09) ($10^{-5}, 10^{-2}$)
USPS	(90.26,2.65) ($10^{-3}, 2^1$)	(91.21,0.64) ($10^{-5}, 10^{-2}, 2^3$)	(56.79,1.77) ($10^{-3}, 100$)	(81.26,0.08) ($10^{-1}, 10^5$)	(86.94,0.07) ($10^{-1}, 10^5, 1.5$)	(90.05,0.58) (0.01)	(84.58,0.45) (10^{-1})	(91.22,0.09) ($10^{-5}, 10^{-1}$)
Yale	(82.30,1.56) ($10^5, 2^3$)	(82.09,0.82) ($10^1, 10^{-5}, 2^3$)	(54.03,3.52) ($10^0, 500$)	(76.42,0.85) ($10^{-1}, 10^5$)	(80.13,0.44) ($10^{-3}, 10^1, 1.9$)	(83.31,1.45) (0.2)	(78.11,1.06) (10^2)	(85.25,1.66) ($10^1, 10^5$)
ORL	(99.60,0.52) ($10^{-3}, 2^3$)	(99.75,0.37) ($10^1, 10^{-5}, 2^3$)	(50.70,5.91) ($10^3, 50$)	(96.48,0.75) ($10^{-3}, 10^1$)	(99.40,0.34) ($10^{-3}, 10^1, 1.3$)	(99.20,0.63) (0.01)	(97.70,0.67) (10^{-5})	(99.80,0.42) ($10^{-5}, 10^{-2}$)
Avg.Acc	92.97	93.26	53.44	87.21	90.59	92.09	89.34	93.96
Avg.rank	2.75	2.25	8.00	7.00	4.75	4.25	5.50	1.50

Table 7: Optimal F1 scores and optimal parameter results for each method on four image datasets.

Datasets	TSVM (F1,Std)(%) (c_2, σ)	CL_1 FRTEB SVM (F1,Std)(%) (c_1, c_2, σ)	CL_1 FRTEL M (F1,Std)(%) (c_2, L)	LINEX-TSVM (F1,Std)(%) (c_1, c_2)	$CL_{2,p}$ -LSTSVM (F1,Std)(%) (c_2, ϵ, p)	ν -FRSQSSVM (F1,Std)(%) (ν)	LSQTSVM (F1,Std)(%) (c_2)	CL_1 QTSVM (F1,Std)(%) (c_1, c_2)
COIL20	(99.81,0.10) ($10^5, 2^3$)	(100.00,0.00) ($10^1, 10^{-5}, 2^3$)	(48.50,4.07) ($10^{-5}, 40$)	(94.25,0.32) ($10^{-1}, 10^5$)	(95.92,0.25) ($10^{-3}, 10^3, 1.9$)	(96.07,0.37) (0.01)	(96.95,0.20) (10^2)	(99.65,0.09) ($10^{-5}, 10^{-1}$)
USPS	(87.83,2.98) ($10^{-3}, 2^1$)	(88.74,1.05) ($10^{-5}, 10^{-2}, 2^3$)	(NaN,NaN) (\cdot, \cdot)	(75.04,0.07) ($10^1, 10^3$)	(83.89,0.08) ($10^{-1}, 10^3, 1.9$)	(87.93,0.77) (0.01)	(80.41,0.81) (10^{-1})	(89.45,0.12) ($10^{-5}, 10^{-1}$)
Yale	(79.05,2.03) ($10^3, 2^3$)	(81.08,2.27) ($10^4, 10^{-5}, 2^3$)	(NaN,NaN) (\cdot, \cdot)	(79.19,0.69) ($10^{-1}, 10^5$)	(71.99,1.58) ($10^{-5}, 10^5, 1.9$)	(81.56,3.31) (0.2)	(77.38,1.19) (10^2)	(83.93,2.22) ($10^1, 10^5$)
ORL	(99.78,0.49) ($10^{-3}, 2^5$)	(99.86,0.45) ($10^1, 10^{-5}, 2^3$)	(NaN,NaN) (\cdot, \cdot)	(97.62,0.42) ($10^1, 10^5$)	(98.09,0.58) ($10^{-5}, 10^3, 1.3$)	(99.11,0.71) (0.01)	(97.30,1.34) (10^{-5})	(99.94,0.19) ($10^{-5}, 10^{-2}$)
Avg.F1	91.62	92.40	NaN	85.53	87.47	91.17	88.01	93.24
Avg.rank	3.50	2.00	8.00	6.00	5.75	3.50	5.75	1.50

4.3. Robustness analysis

In this subsection, to validate that our CL_1 QTSVM model is insensitive to outliers on the benchmark datasets, we select six small-scale benchmark datasets for numerical experiments. As shown in Figure 6, the additive noise ratios are 0%, 5% and 10%, 15%, 20%, 25% and 30%, respectively. As can

Table 8: Running time of each method on four image datasets.

Datasets	TSVM (Time)(s)	CL_1 FRTBSVM (Time)(s)	CL_1 FRTELm (Time)(s)	LINEX-TSVM (Time)(s)	$CL_{2,p}$ -LSTSVM (Time)(s)	ν -FRSQSSVM (Time)(s)	LSQTSVM (Time)(s)	CL_1 QTSVM (Time)(s)
COIL20	(90.76)	(36.40)	(8.19)	(8.11)	(161.22)	(1198.97)	(199.72)	(98.43)
USPS	(1089.48)	(5363.28)	(69.73)	(181.67)	(467.56)	(11838.59)	(65.08)	(100.83)
Yale	(0.62)	(0.31)	(16.29)	(2.69)	(3.25)	(139.14)	(23.60)	(34.20)
ORL	(0.27)	(0.21)	(1.11)	(2.57)	(3.93)	(88.65)	(14.65)	(35.31)
Avg.Time	295.28	1350.05	23.83	48.76	158.99	3316.34	75.76	67.19

be seen from the results, the classification performance of our CL_1 QTSVM model is less affected by the increase of noise ratios. Specifically, on the datasets Australian, CMC, Sonar, WBC, Yeast (2 vs. 8) and Robotnavig, the classification performance of the CL_1 QTSVM model slightly outperforms that of the rest of the compared methods. In particular, on the dataset Robotnavig, the robustness of the CL_1 QTSVM model is higher than that of the remaining compared methods. However, on the CMC, Australian and WBC datasets, the classification performance of our CL_1 QTSVM model is comparable to that of the CL_1 FRTBSVM model. It should be noted that our CL_1 QTSVM model has much better classification results on these six datasets compared with the traditional TSVM and LSQTSVM models. From the analysis of the above results, it can be seen that our CL_1 QTSVM model has some advantages.

Our CL_1 QTSVM model outperforms other state-of-the-art methods for the following reasons: (1) Capped L_1 -norm is introduced into CL_1 QTSVM model, which effectively reduces the influence of outliers on our model. (2) The introduction of L_2 -regularization term improves the generalization ability of our model. (3) The designed iterative algorithm can have the ability to solve CL_1 QTSVM model, which leads to better performance. (4) Our CL_1 QTSVM model is kernel-free, which effectively solves the difficulty of selecting the kernel functions and kernel parameters of the comparative kernel methods on certain datasets.

4.4. Parameter sensitivity analysis

This subsection mainly analyzes the relationship between the regularization parameter c_1 and the penalty parameter c_2 of our CL_1 QTSVM model with the classification accuracy. Figure 7 shows the results on six benchmark datasets. The results are analyzed as follows: on the dataset Australian, it can be seen that our CL_1 QTSVM model is insensitive to the regularization parameter c_1 , but is more sensitive to the penalty parameter c_2 ; when $c_2 \in (10^{-5}, 10^0)$, our CL_1 QTSVM model can obtain the highest accuracy.

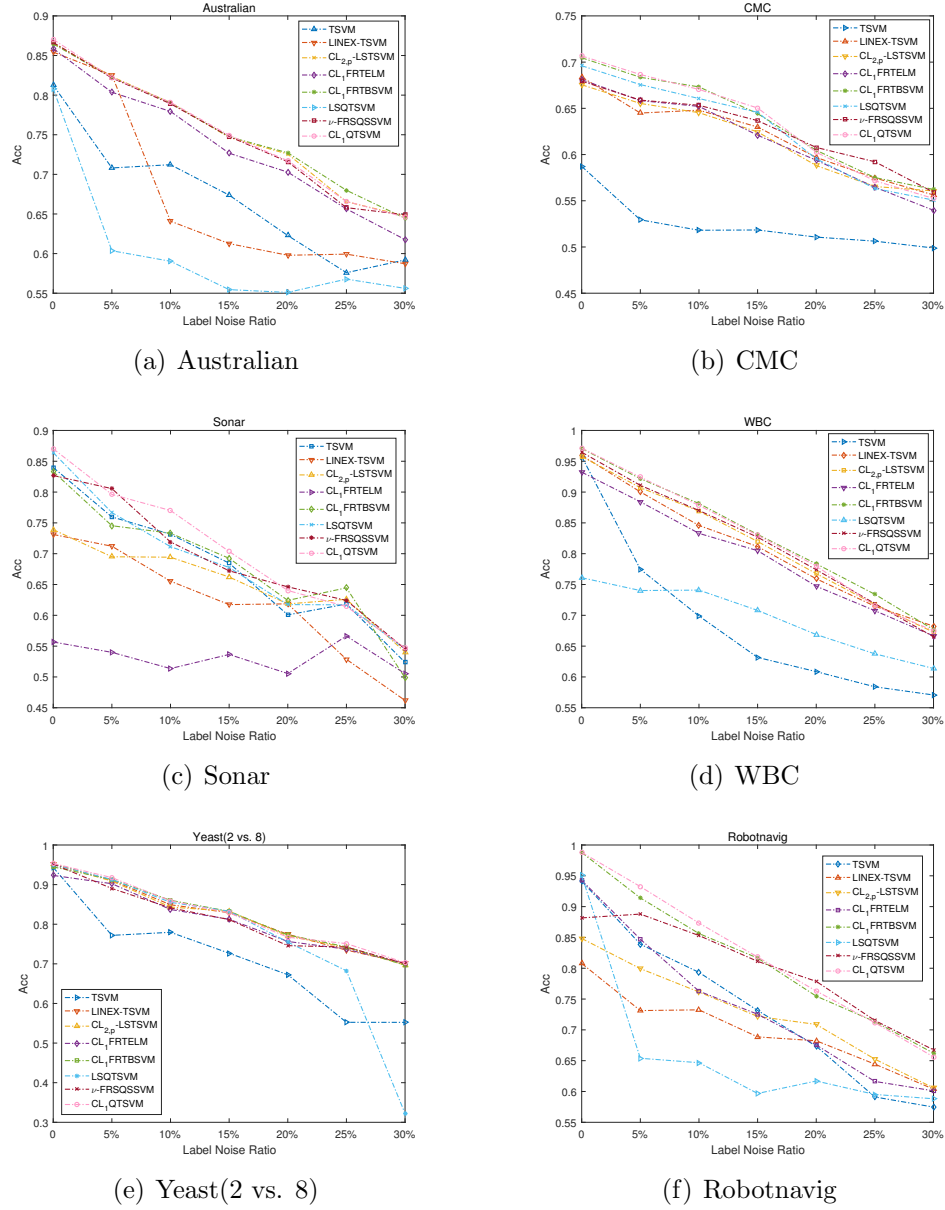


Figure 6: Comparison of classification performance by methods with different label noises.

On the dataset Climate-simulation, our CL_1 QTSVM model is insensitive to both parameters c_1 and c_2 . On the Ionosphere, our CL_1 QTSVM model is insensitive to the parameter c_1 ; However, our CL_1 QTSVM model can find the optimal parameter when $c_2 \in (10^{-5}, 10^{-3})$. On the dataset Robot-navig, our CL_1 QTSVM model finds the optimal parameter combinations when $c_2 \in (10^{-5}, 10^0)$ and $c_1 \in (10^{-5}, 10^{-3})$. On the dataset Sonar and Yeast (2 vs. 8), our CL_1 QTSVM model is insensitive to the parameter c_1 ; but when $c_2 \in (10^{-5}, 10^0)$, the CL_1 QTSVM model finds the optimal parameter combination. Based on the above analysis, we can get the following conclusions: (1) Our CL_1 QTSVM model is insensitive to the parameter c_1 , which can be set to the range of $c_1 \in (10^{-5}, 10^0)$. (2) In order to obtain better classification performance, the optimal parameter range for parameter c_2 is $c_1 \in (10^{-5}, 10^0)$.

4.5. Convergence analysis

Figure 8 shows the objective function value versus the number of iterations for our CL_1 QTSVM method on the six benchmark datasets. Note that the objective function value is the sum of the objective function values of our optimization problem (15) and (16). In the convergence analysis experiments, 90% of the data points in each benchmark dataset are randomly selected as the training set, and the remaining 10% of the points are used as the test set. From the Figure 8 we can observe that the objective function value decreases rapidly and converges within 10 iteration steps. Therefore, these convergence analysis results effectively validate the convergence and effectiveness of our proposed CL_1 QTSVM model.

4.6. Non-parametric statistical test

In this subsection, we use the Nemenyi post hoc test (García et al., 2010) to further validate the differences between the CL_1 QTSVM model and other comparative state-of-the-art methods. The principle of this test is that if the difference between the mean ranks of the two algorithms is greater than the calculated critical difference (CD), we consider the two algorithms to be significantly different. Otherwise, there is no significant difference between the two algorithms. In addition, the CD value is calculated as follows

$$CD = q_\alpha(k) \times \sqrt{\frac{k(k+1)}{6N}}, \quad (65)$$

where $\alpha = 0.05$, and we have $q_\alpha = 3.0310$.

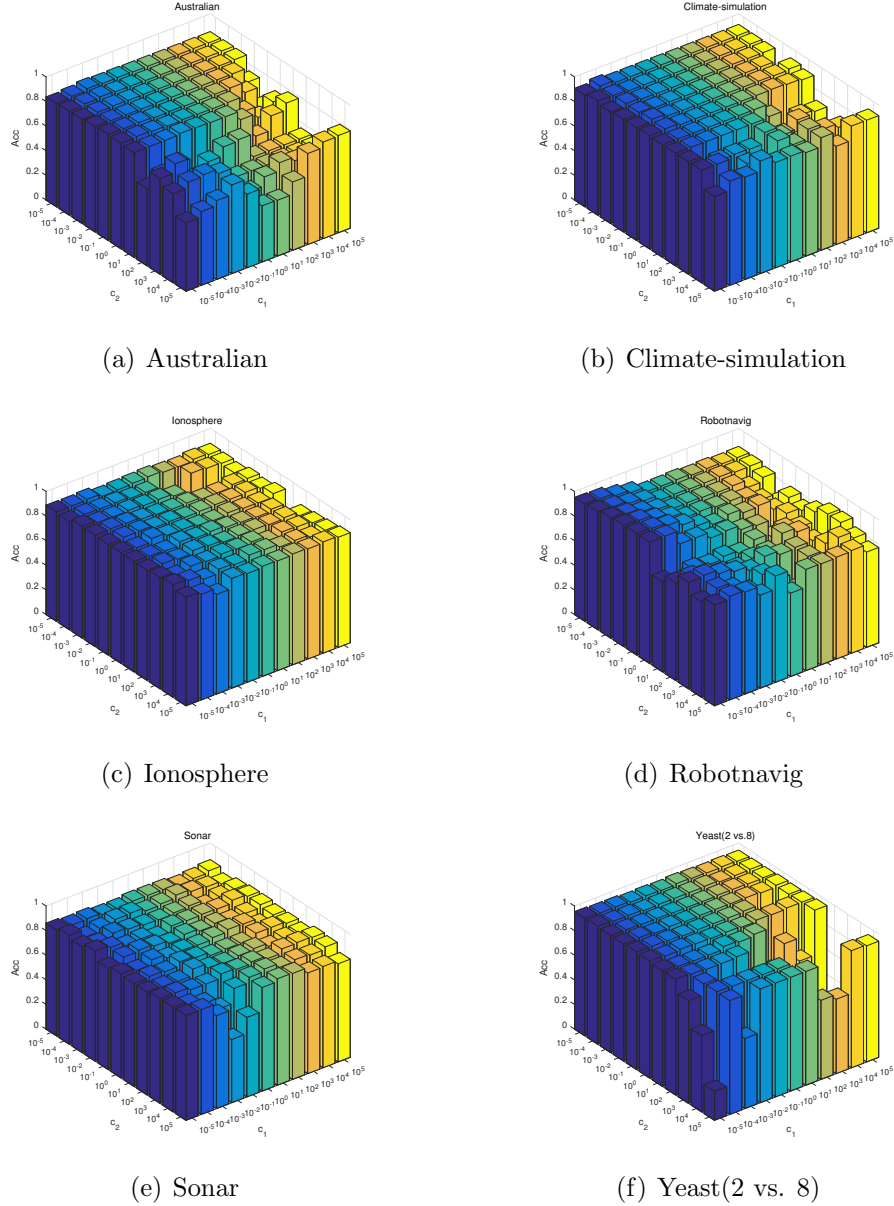


Figure 7: Accuracy variation of CL1QT-SVM model with different hyperparameters.

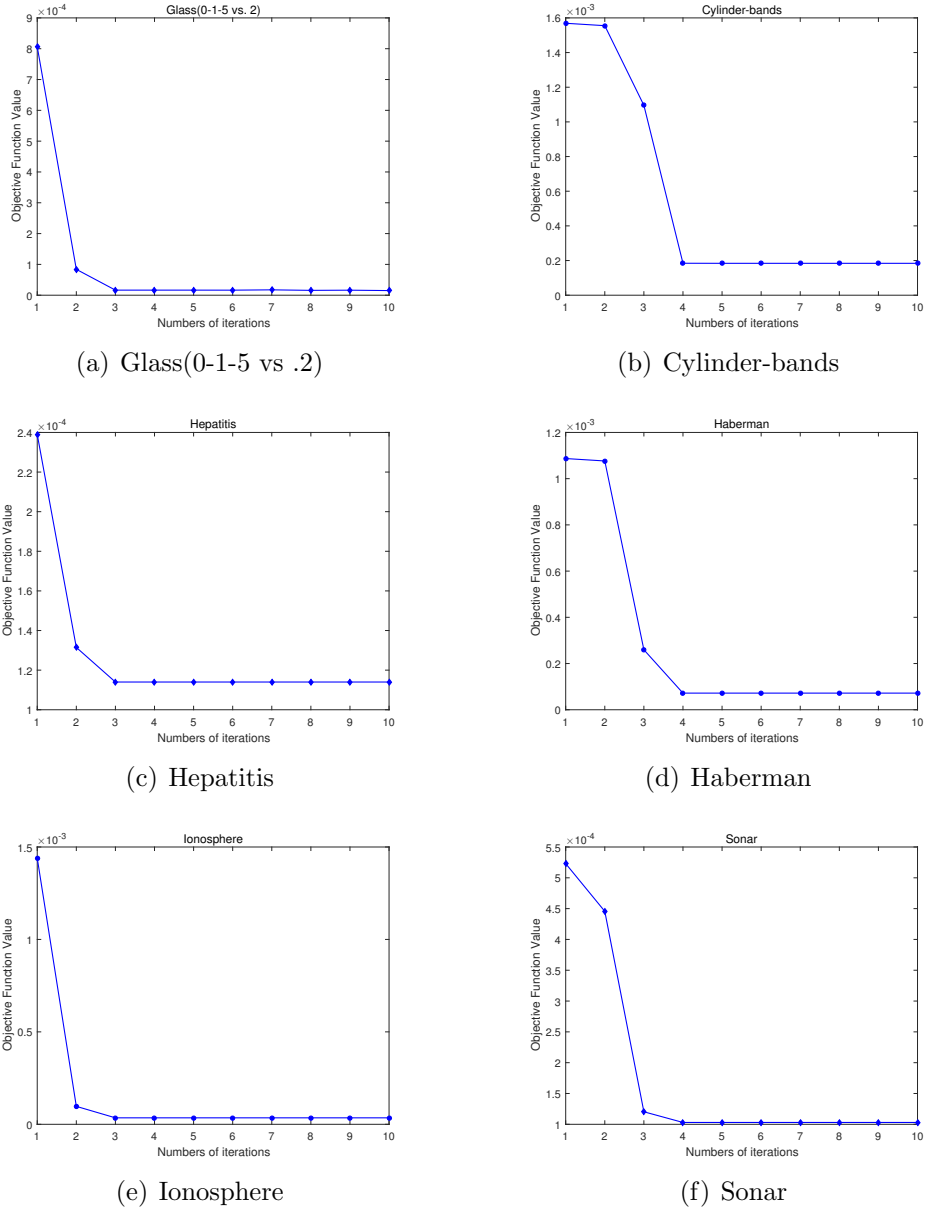


Figure 8: Convergence of the CL_1 QTSVM model on 6 benchmark datasets.

As shown in Figure (9), there is no significant difference between the methods connected by the red line. Based on the experimental results on the synthetic dataset in Table 3, Figure (9)(a) demonstrates the results of the corresponding Nemenyi post hoc test. From Figure (9)(a), it can be seen that the average classification results of the proposed CL_1 QTSVM model on the nine synthetic datasets are not significantly different from those of CL_1 FRTBSVM, TSVM, and LSQTSVM; However, there is a significant difference between the classification performance of our CL_1 QTSVM model and that of the remaining four comparison methods. In addition, based on the experimental results on the benchmark dataset in Table 2, Figure (9)(b) shows the corresponding Nemenyi post-test results. From Figure (9)(b), it can be seen that the classification performance of the proposed CL_1 QTSVM model on the 16 benchmark datasets is not significantly different from that of ν -FRSQSSVM, CL_1 FRTBSVM and $CL_{2,p}$ -LSTSVM, but there is a significant difference between them and the remaining four methods. From the above results, we can see that our CL_1 QTSVM model is effective in dealing with synthetic data with outliers, benchmark data and nonlinear data.

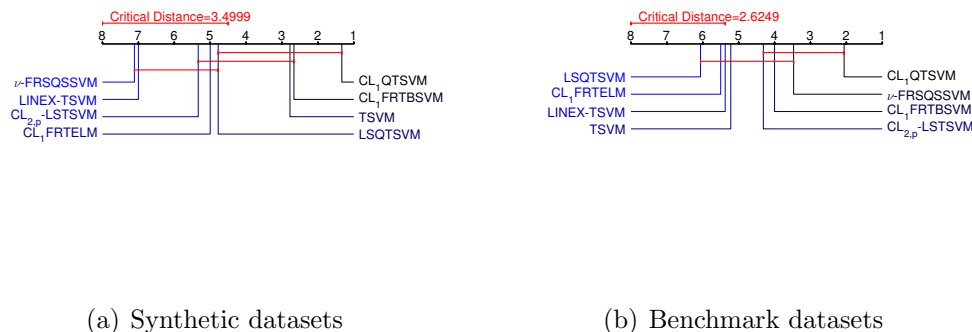


Figure 9: Nemenyi post hoc tests on synthetic and benchmark datasets.

5. Conclusion

In this paper, a capped L_1 -norm kernel-free quadratic support vector machine (CL_1 QTSVM) is proposed from the perspectives of distance norms and kernel-free techniques. First, a non-smooth but bounded and symmetric capped L_1 -norm distance measure is introduced to improve the robustness of

the model to outliers. Meanwhile, the introduction of the L_2 -norm regularization term improves the generalization ability of the model. In addition, in order to avoid the time-consuming problem of selecting the appropriate kernel functions and kernel parameters for the traditional twin support vector machine model on some real datasets, this paper extends the model to a kernel-free version by utilizing the kernel-free technique, where only two quadratic hypersurfaces need to be found for the proposed CL_1 QTSVM model. For the established non-differentiable optimization problem, the original problem is equivalently transformed by reweighting technique, and an efficient iterative algorithm is constructed for the transformed optimization problem. In the theory section, the convergence, time complexity and existence of local optimal solutions of the designed iterative algorithm are analyzed in detail.

In the numerical experiments, the experiments on synthetic dataset, benchmark dataset and image recognition dataset show that the CL_1 QTSVM model has certain advantages in terms of classification performance, robustness and computation time. In the future, we can extend the CL_1 QTSVM model to multi-view learning, multi-classification problems and clustering problems. Similarly, deep learning and functional data classification are also directions that can be considered.

Acknowledgements

This work is supported by the National Natural Science Foundation of China (No.12061071) and Xinjiang Key Laboratory of Applied Mathematics (No.XJDX1401).

Conflict of interest

The authors declare that they have no conflict of interest.

References

- Bai, Y., Han, X., Chen, T., Yu, H., 2015. Quadratic kernel-free least squares support vector machine for target diseases classification. *Journal of Combinatorial Optimization* 30, 850–870.
- Borah, P., Gupta, D., 2020. Functional iterative approaches for solving support vector classification problems based on generalized huber loss. *Neural Computing and Applications* 32 (13), 9245–9265.

Brown, M. P., Grundy, W. N., Lin, D., Cristianini, N., Sugnet, C. W., Furey, T. S., Ares Jr, M., Haussler, D., 2000. Knowledge-based analysis of microarray gene expression data by using support vector machines. *Proceedings of the National Academy of Sciences* 97 (1), 262–267.

Chandra, S., Khemchandani, R., 2007. Twin support vector machines for pattern classification. *IEEE Transactions on Pattern Analysis and Machine Intelligence* 29 (5), 905–910.

Cortes, C., Vapnik, V., 1995. Support vector networks. *Machine learning* 20, 273–297.

Gao, D. Y., Yu, H., 2008. Multi-scale modelling and canonical dual finite element method in phase transitions of solids. *International Journal of Solids and Structures* 45 (13), 3660–3673.

Gao, Q.-Q., Bai, Y.-Q., Zhan, Y.-R., 2019. Quadratic kernel-free least square twin support vector machine for binary classification problems. *Journal of the Operations Research Society of China* 7, 539–559.

Gao, Z., Fang, S.-C., Gao, X., Luo, J., Medhin, N., 2021a. A novel kernel-free least squares twin support vector machine for fast and accurate multi-class classification. *Knowledge-Based Systems* 226, 107123.

Gao, Z., Fang, S.-C., Luo, J., Medhin, N., 2021b. A kernel-free double well potential support vector machine with applications. *European Journal of Operational Research* 290 (1), 248–262.

Gao, Z., Wang, Y., Huang, M., Luo, J., Tang, S., 2022. A kernel-free fuzzy reduced quadratic surface ν -support vector machine with applications. *Applied Soft Computing* 127, 109390.

García, S., Fernández, A., Luengo, J., Herrera, F., 2010. Advanced non-parametric tests for multiple comparisons in the design of experiments in computational intelligence and data mining: Experimental analysis of power. *Information Sciences* 180 (10), 2044–2064.

Goh, K.-S., Chang, E.-Y., Li, B., 2005. Using one-class and two-class svms for multiclass image annotation. *IEEE transactions on Knowledge and Data Engineering* 17 (10), 1333–1346.

Gupta, D., Hazarika, B. B., Berlin, M., 2020. Robust regularized extreme learning machine with asymmetric huber loss function. *Neural Computing and Applications*, 1–28.

Hearst, M. A., Dumais, S. T., Osuna, E., Platt, J., Scholkopf, B., 1998. Support vector machines. *IEEE Intelligent Systems and their applications* 13 (4), 18–28.

Huang, L.-W., Shao, Y.-H., Zhang, J., Zhao, Y.-T., Teng, J.-Y., 2019. Robust rescaled hinge loss twin support vector machine for imbalanced noisy classification. *IEEE Access* 7, 65390–65404.

Kumar, M. A., Gopal, M., 2009. Least squares twin support vector machines for pattern classification. *Expert systems with applications* 36 (4), 7535–7543.

Luo, J., Fang, S.-C., Deng, Z., Guo, X., 2016. Soft quadratic surface support vector machine for binary classification. *Asia-Pacific Journal of Operational Research* 33 (06), 1650046.

Ma, J., 2020. Capped l1-norm distance metric-based fast robust twin extreme learning machine. *Applied Intelligence* 50 (11), 3775–3787.

Ma, J., Yang, L., Sun, Q., 2020. Capped l1-norm distance metric-based fast robust twin bounded support vector machine. *Neurocomputing* 412, 295–311.

Ma, S., Cheng, B., Shang, Z., Liu, G., 2018. Scattering transform and lsptsvm based fault diagnosis of rotating machinery. *Mechanical Systems and Signal Processing* 104, 155–170.

Moosaei, H., Ganaie, M., Hladík, M., Tanveer, M., 2023. Inverse free reduced universum twin support vector machine for imbalanced data classification. *Neural Networks* 157, 125–135.

Nie, F., Huang, Y., Wang, X., Huang, H., 2014. New primal svm solver with linear computational cost for big data classifications. in: *International Conference on Machine Learning* (II-505).

Noble, W.-S., 2004. Support vector machine applications in computational biology. *Kernel Methods in Computational Biology* 71, 92.

Shao, Y.-H., Zhang, C.-H., Wang, X.-B., Deng, N.-Y., 2011. Improvements on twin support vector machines. *IEEE Transactions on Neural Networks* 22 (6), 962–968.

Si, Q., Yang, Z., Ye, J., 2023. Symmetric linex loss twin support vector machine for robust classification and its fast iterative algorithm. *Neural Networks*.

Tanveer, M., Sharma, A., Suganthan, P.-N., 2019. General twin support vector machine with pinball loss function. *Information Sciences* 494, 311–327.

Wang, C., Ye, Q., Luo, P., Ye, N., Fu, L., 2019. Robust capped l1-norm twin support vector machine. *Neural Networks* 114, 47–59.

Wang, H., Yu, G., Ma, J., 2023. Capped l_2 , p -norm metric based on robust twin support vector machine with welsch loss. *Symmetry* 15 (5), 1076.

Wang, Y.-F., Yu, G.-L., & Ma, J., 2022. Capped linex metric twin support vector machine for robust classification. *Sensors* 22 (17), 6583.

Wu, M.-J., Liu, J.-X., Gao, Y.-L., Kong, X.-Z., Feng, C.-M., 2017. Feature selection and clustering via robust graph-laplacian pca based on capped l_1 -norm. In: 2017 IEEE international conference on Bioinformatics and Biomedicine (BIBM). pp. 1741–1745.

Xia, Y., Sheu, R.-L., Fang, S.-C., Xing, W., 2014. Double well potential function and its optimization in the n-dimensional real space-part ii. *Journal of Industrial and Management Optimization*.

Xiang, S., Nie, F., Meng, G., Pan, C., Zhang, C., 2012. Discriminative least squares regression for multiclass classification and feature selection. *IEEE transactions on neural networks and learning systems* 23 (11), 1738–1754.

Xie, X., Li, Y., Sun, S., 2023a. Deep multi-view multiclass twin support vector machines. *Information Fusion* 91, 80–92.

Xie, X., Sun, F., Qian, J., Guo, L., Zhang, R., Ye, X., Wang, Z., 2023b. Laplacian l_p norm least squares twin support vector machine. *Pattern Recognition* 136, 109192.

Xie, X., Xiong, Y., 2022. Generalized multi-view learning based on generalized eigenvalues proximal support vector machines. *Expert Systems with Applications* 194, 116491.

Yan, H., Ye, Q., Zhang, T., Yu, D.-J., Yuan, X., Xu, Y., Fu, L., 2018. Least squares twin bounded support vector machines based on l1-norm distance metric for classification. *Pattern recognition* 74, 434–447.

Yang, Y., Xue, Z., Ma, J., Chang, X., 2023. Robust projection twin extreme learning machines with capped l1-norm distance metric. *Neurocomputing* 517, 229–242.

Yuan, C., Yang, L., 2021. Capped l2, p-norm metric based robust least squares twin support vector machine for pattern classification. *Neural Networks* 142, 457–478.

Zheng, X.-H., Zhang, L., Yan, L.-L., 2021. Ctsvm: a robust twin support vector machine with correntropy-induced loss function for binary classification problems. *Information Sciences* 559, 22–45.